Materials Research
Express

INCLUSIVE PUBLISHING
TRUSTED SCIENCE

PURPOSE-LED
PUBLISHING™

PAPER • **OPEN ACCESS**

Surface modification of plasma spraying $A_{l2}O_3$–13 wt% TiO_2 coating by laser remelting technique

To cite this article: Yan Zhou *et al* 2022 *Mater. Res. Express* **9** 056401

View the article online for updates and enhancements.

You may also like

- Effects of Yttrium on the pitting corrosion behavior of 304 stainless steel with coating by laser remelting
Mengnan Liu, Dongxu Chen, Yanan Wang et al.
- Globular to lamellar transition during anomalous eutectic growth
Wei Lei, Cao Yongqing, Lin Xin et al.
- Influences of Feedstocks and Laser Remelting on Erosion Resistance of Al_2O_3-13wt.%TiO_2 Coatings Prepared by Plasma Spraying
Dongsheng Wang and Xinghua Zhou

This content was downloaded from IP address 173.177.195.252 on 26/02/2026 at 16:42

Materials Research Express

PAPER

Surface modification of plasma spraying Al_2O_3–13 wt% TiO_2 coating by laser remelting technique

Yan Zhou[1], **Lifeng Xu**[1], **Haizhong Zheng**[2,*] **and Dongsheng Wang**[1,2,3,4,5,*]

[1] College of Mechanical Engineering, Tongling University, Tongling, People's Republic of China
[2] Jiangxi Key Laboratory of Forming and Joining Technology for Aerospace Components, Nanchang Hangkong University, Nanchang, People's Republic of China
[3] Key Laboratory of Construction Hydraulic Robots of Anhui Higher Education Institutes, Tongling University, Tongling, People's Republic of China
[4] Key Laboratory of Additive Manufacturing of Tongling City, Tongling University, Tongling, People's Republic of China
[5] Engineering Technology Research Center of Semiconductor Packaging Die of Tongling City, Tongling Yuanyi Precision Machinery Co., Ltd, Tongling, People's Republic of China
* Authors to whom correspondence should be addressed.

E-mail: haizhongzheng@126.com **and** wangdongsheng@tlu.edu.cn

Keywords: plasma spraying, laser remelting, Al_2O_3-13 wt%TiO_2 coating, microstructure, properties

OPEN ACCESS

RECEIVED
17 March 2022

REVISED
7 April 2022

ACCEPTED FOR PUBLICATION
25 April 2022

PUBLISHED
6 May 2022

Original content from this work may be used under the terms of the Creative Commons Attribution 4.0 licence.

Any further distribution of this work must maintain attribution to the author(s) and the title of the work, journal citation and DOI.

Abstract

An Al_2O_3–13 wt% TiO_2 composite ceramic coating was prepared on the TiAl alloy surface by plasma spraying and laser remelting combined technique. The morphology, microstructure, and phase composition of the prepared coating were analyzed by scanning electron microscopy, energy disperse spectroscopy, and x-ray diffraction. The bonding strength, microhardness, wear resistance, erosion resistance, and thermal shock resistance of the coating were also tested. Results demonstrated that after processing by laser remelting, the particles on the ceramic coating surface were refined, lamellar structure disappeared, and density increased. A remelting layer basically without crack and other defects was gained. Due to laser remelting, the metastable-phase γ-Al_2O_3 was converted into stable-phase α-Al_2O_3. Influenced by the low thermal conductivity of ceramic materials, remelting of the whole ceramic layer is impossible to realize during laser remelting. The remelted ceramic coating formed the isometric crystal remelting zone with small grain size, sintering zone, and lamellar residual plasma spraying zone. The bonding strength and microhardness of the coating improved significantly after laser remelting, and the wear resistance, erosion resistance, and thermal shock resistance were significantly superior to those of the original plasma spraying layer. Laser remelting specimens still represented typical brittle erosion characteristics. Cracks initiated and expanded on near surface, finally leading to breakage of the remelting layer, mainly manifested by grain peeling. With respect to thermal shock failure mode, the corner peeling is the major failure mode of the ceramic coating after plasma spraying. Differently, corner peeling and considerable local peelings were found at the center of the ceramic coating after laser remelting. The influences of laser remelting on the thermal shock performances of the coating are mainly manifested as the decreased initial failure resistance, decelerated crack expansion, and changes in failure modes of the coating.

1. Introduction

Although ceramic materials have excellent wear resistance, corrosion resistance, heat tolerance and high-temperature oxidation resistance, their applications are restricted to some extent due to great brittleness, poor fatigue resistance, high sensitivity to stress and cracks, and difficult processing [1–4]. On the one hand, ceramic coating technique on metal surface can organically combine characteristics of the base metal and the ceramic coating on metal surface and develop the comprehensive advantages of two materials. On the other hand, ceramic coating technique can meet the needs of structural and environmental performances and thereby

© 2022 The Author(s). Published by IOP Publishing Ltd

acquire quite ideal composite structures. As a result, applying a protective ceramic coating is an effective means to improve the performances of metal surface [5–10].

Plasma spraying is one of the most common ceramic coating technologies on metal surface. Nevertheless, the characteristics of plasma spraying technology determine if the coating has typical lamellar structures, relatively high non-equilibrium, and porosity. Mechanical bonding is the major form of interface bonding. Consequently, coating formed by plasma spraying is difficult to adapt to relatively poor working environment. Therefore, the application scope and service life of plasma spraying are restricted [11–15]. Laser remelting of the plasma spraying layer provides a new pathway to solve this technological challenge. It could eliminate the lamellar structure, most pores and oxide inclusions of the coating, forming a uniform and dense ceramic coating and assuring the performances of the coating. Therefore, the service life of workpieces is prolonged [16–64]. According to existing studies, laser remelting could improve the properties of plasma spraying layer, including structure [40–47], bonding strength [48, 49], wear resistance [46, 50–55], corrosion performance [55, 56], thermal corrosion [57–59], oxidization performance [47, 60], thermal shock performances [61–63], and erosion resistance [64].

Al_2O_3 is the most important and widely used anti-wear ceramic coating material. It is also a kind of ceramic material commonly used in plasma spraying technology, but the toughness of pure Al_2O_3 is insufficient. Adding an appropriate amount of TiO_2 (3%–40%) into Al_2O_3 ceramics to make Al_2O_3–TiO_2 composites can improve the toughness, compactness and bonding strength of Al_2O_3 ceramics, which is conducive to the further improvement of wear resistance and erosion resistance [65–68]. Common Al_2O_3–TiO_2 composites include Al_2O_3–3 wt% TiO_2 [69, 70], Al_2O_3–8 wt% TiO_2 [71, 72], Al_2O_3–13 wt% TiO_2 [73–75], and Al_2O_3–40 wt% TiO_2 [76–79], etc, among which Al_2O_3–13 wt% TiO_2 ceramic has a good coordination in hardness and toughness, and its application is the most common [73–75].

In this study, the ceramic powder of Al_2O_3-13 wt%TiO_2 (AT13) was used as the raw material, and a composite ceramic coating was prepared on the TiAl alloy surface by plasma spraying method. The prepared coating was processed by laser remelting. The morphology, microstructure, and phase composition of the prepared coating were investigated and characterized by scanning electron microscopy (SEM), energy disperse spectroscopy (EDS), and x-ray diffraction (XRD). Moreover, a comprehensive performance test was carried out to systematically investigate the influences of laser remelting on the microstructure, bonding strength, microhardness, wear resistance, erosion resistance, and thermal shock resistance of the coating.

2. Experimental method

2.1. Experimental materials

γ-TiAl-based alloys (TAC-2) melted by the Institute of High Temperature Materials, Central Iron and Steel Research Institute, was used as the base material in this experiment. Three dimensions were applied, including Φ25 mm $\times$ 8 mm (bonding strength and thermal shock specimens), 10 mm $\times$ 10 mm $\times$ 8 mm (wear test specimens) and 20 mm $\times$ 20 mm $\times$ 8 mm (erosion specimens). The nominal chemical composition was Ti-46.5Al-2.5V-1Cr (at.%). The transition layer used the NiCoCrAl superalloy powder (KF-113A) with granularity ranging from $-$140 meshes to $+$325 meshes and dispersed by Y_2O_3. It was produced by the Institute of Metal Materials, Beijing General Research Institute of Mining and Metallurgy. The nominal chemical composition was Ni-20Co-18Cr-15Al-2Y_2O_3 (wt%). The transition layer is mainly to decrease the great differences in the physical properties between the ceramic coating and the base metal to relax stress and avoid cracking of the coating. This also strengthens the bonding force between the coating and the base. The commercial AT13 composite ceramic powder with granularity of 15–45 μm and irregular ordinary mechanical breakages, produced by Shenyang Ronghua, was used as the ceramic material. SEM morphologies of KF-113A and AT13 powders are shown in figure 1.

2.2. Experimental apparatus and technologies

The KF-113A transition layer and AT13 ceramic layer were prefabricated by plasma spraying with the use of 3710 plasma spraying system (Praxair, USA). Preprocessing of specimens, including polishing, de-oiling, and sand blasting, was performed before spraying. The quality of plasma-sprayed coating is affected by the interaction of many factors, such as powder particle size and morphology, type and flow of working gas, spraying power, powder carrier gas, spraying distance, traverse speed of spray gun or workpiece, which makes the coating quality difficult to control [80]. Previous studies have shown that the influences of main factors on the sprayed coating are spraying distance, current, primary gas flow, secondary gas flow and so on [71, 81]. After preliminary experiments, the relatively optimized plasma spraying technological parameters are listed in table 1.

Laser cladding process can be divided into coaxial powder feeding laser cladding, pre-placed laser cladding, off-axis powder feeding laser cladding, and wire feeding laser cladding according to the cladding material supply

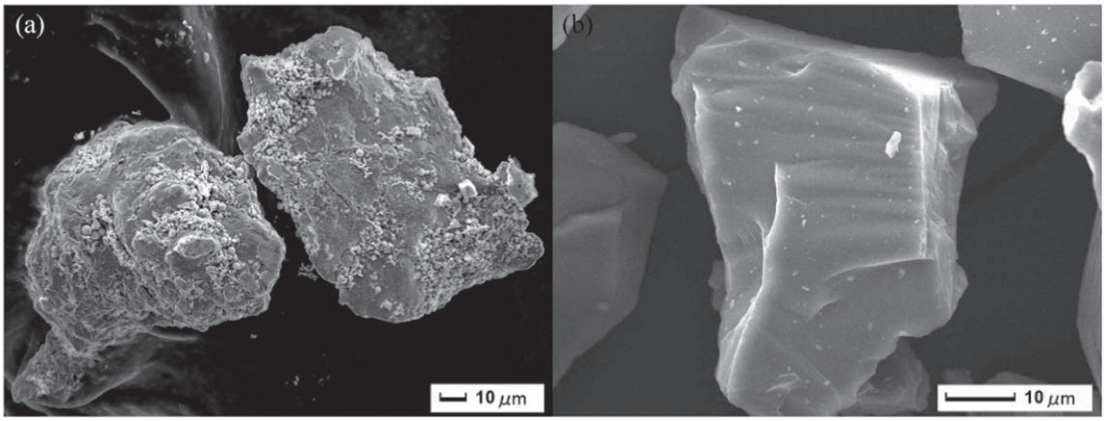


Figure 1. SEM morphologies of powder: (a) KF-113A, and (b) AT13.

Table 1. Plasma spraying parameters.

Process parameters	KF-113A	AT13
Current	710 A	850 A
Voltage	42 V	42 V
Primary gas (Ar)	65 PSI	45 PSI
Secondary gas (He)	115 PSI	140 PSI
Powder carrier gas (Ar)	45 PSI	45 PSI
Powder feed rate	2 r·min^{-1}	3 r·min^{-1}
Spray distance	110 mm	110 mm
Traverse speed	100 mm·s^{-1}	100 mm·s^{-1}
Coating thickness	~ 100 μm	~350 μm

method. Laser cladding of thermal-sprayed pre-placed coating is also known as laser remelting. Technological parameters of laser remelting (such as laser power, scanning speed, spot size, etc) and coating (such as coating thickness, thermophysical parameters of materials, laser absorption rate of coating surface, etc) affecting coating performance, especially laser power is one of important operational parameter. According to the working medium, the common lasers used for laser cladding/remelting can divided into gas laser, solid-state laser, semiconductor laser, fiber laser, etc In this study, the SLCF-X12 $\times$ 25 CO_2 laser machine (Shanghai Tuanjie Prima laser equipment Co., Ltd, China) was applied in laser remelting, and Ar protection was used during remelting. Currently, the major problems in laser remelting ceramic coating are high coating brittleness and great cracking tendency, which considerably restrict its scope of application in key components. Thus, cracking inhibition in laser remelting is of great realistic significance to the application of laser remelting technology in production. In this paper, there are no other measures to reduce the laser remelting Al_2O_3–13 wt% TiO_2 ceramic coating. Relatively low laser power and energy density were chosen for the remelting process to decrease defects (e.g., cracks) of the remelting layer. Through tests, relatively optimal technological parameters of laser remelting were gained as follows: laser power $=$ 650 W; 5 mm $\times$ 3 mm rectangular spot, laser scanning along 3 mm side of the spot, scanning speed $=$ 1200 mm·min^{-1}, and amount of overlapping $=$ 20%. The prepared typical samples are shown in figure 2.

2.3. Microstructure and performance analysis of specimens

The surface, cross section, and sectional morphology of the coating were observed by JSM-7100F (JEOL) field-emission SEM, and relevant mechanisms were discussed. The phases of the coating were analyzed by XRD on the D/max2500 x-ray diffractometer (Rigaku, Japan). The XRD test conditions were as follows: copper target (Kα, $\lambda = 0.154, 178$ nm), electron accelerating voltage $=$ 50 kV, current $=$ 200 mA, scanning speed $= 4^\circ$ min^{-1}, and step width $= 0.02^\circ$.

The preparation of tensile specimens is shown in figure 3(a). Specimens were placed between two mating plates, bonded by E-7 super glue (Shanghai Synthetic Resin Research Institute, tensile strength $>$70 MPa), and then solidified in a drying oven. The clamp, which fixes the mating plates, is shown in figure 3(b). This clamp could assure that the mating plates were coaxial with the specimens in the bonding process. The stretching equipment, WE-100 hydraulic universal tester, is shown in figure 3(c). On the tester, the mating plates were

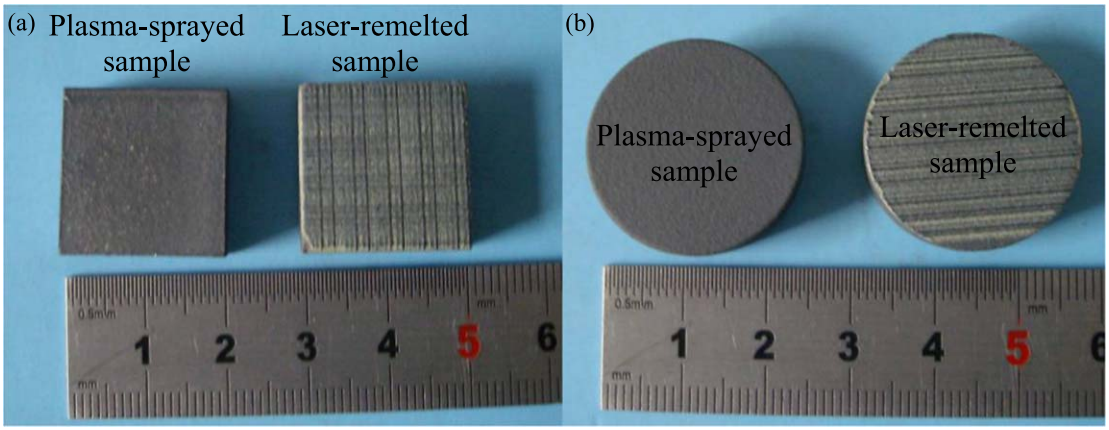


Figure 2. Pictures of typical specimens: (a) erosion specimen, and (b) thermal shock specimens.

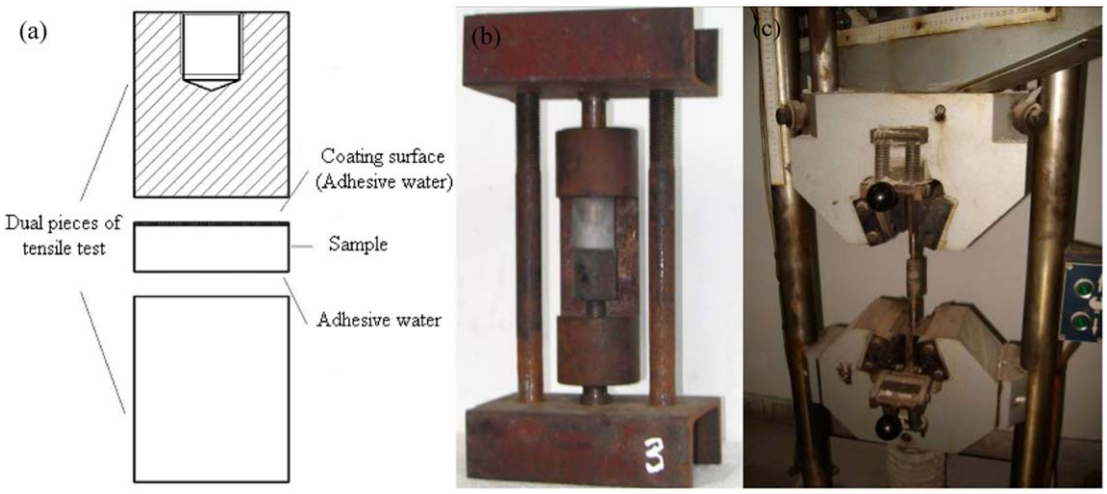


Figure 3. Tensile test of specimens: (a) preparation of tensile test specimens, (b) fixing clamp, and (c) stretching equipment.

stretched away slowly and continuously throughout the loading process (loading speed was controlled at 10 kN·min^{-1}) until the mating plates were pulled apart. The separation loads were recorded. In accordance with the surface area of specimens and the measured loads, it could be calculated as follows:

$$\sigma_F = P/S \tag{1}$$

where σ_F is the normal bonding strength (MPa) of the coating, P is the separation loads of specimens (N), and S is the surface area of samples (mm^2).

The surface area of specimens were substituted into the following formula:

$$\sigma_F = 4P/\pi d^2 \tag{2}$$

where d is diameter of specimens.

The microhardness of the coating was tested using the HXD-1000TC microhardness meter. During the measurement, loads were set to 100 g and kept for 15 s. Dry sliding wear test under room temperature was performed on the MM200 ring-block frictional wear tester. The wear test principle and test process are shown in figure 4. The d 40 mm (outer hole) $\times$ d 16 mm (inner hole) $\times$ 10 mm (thickness) mating grinding rings used the steel 45# after quenching-low tempering, with a hardness of 53 $\pm$ 3 HRC. In the test, the normal load was set to 100 N and the rotating speed of the mating grinding rings was 100 r·min^{-1}. Moreover, B3200S ultrasonic cleaners were used to clean specimens and the FA1004 analytical balance with a weight sensitivity of 10^{-4} g was applied to weight wearing weight loss of specimens (all results were the mean values of three specimens).

Solid particle erosion test was carried out on the erosion tester, which was reconstructed using the sand blasting machine. The working principle is shown in figure 5(a). By using compressive air as the impetus, the erosion tester drove abrasive particles to be ejected onto the coating surface of specimens, thus realizing the

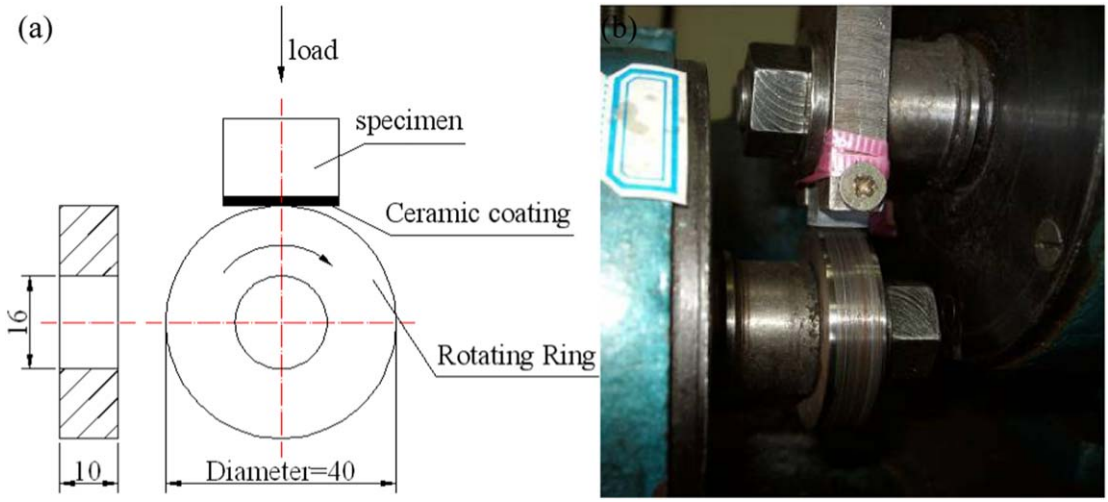


Figure 4. (a) Wear test principle, and (b) west test process.

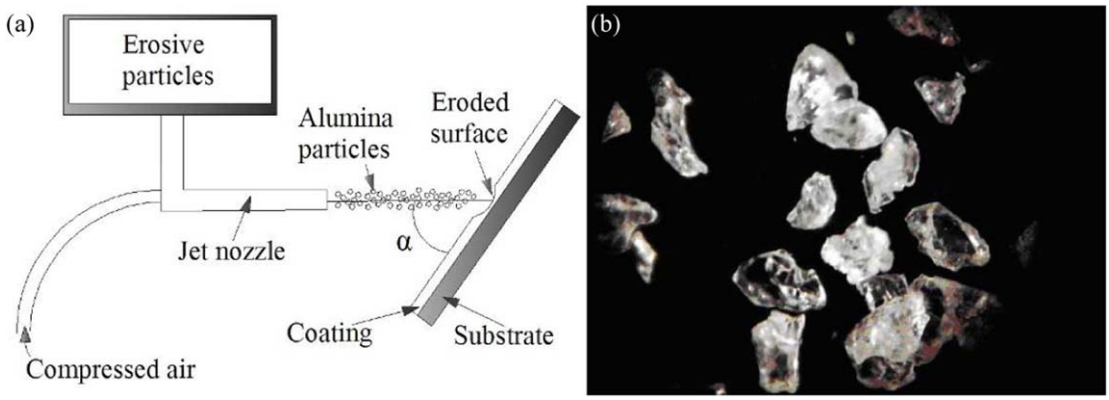


Figure 5. (a) Schematic of erosion test, and (b) optical pictures of abrasive particles.

microscopic cutting and impact onto the specimen surface. The erosion test was performed under room temperature. The natural corundum (Al_2O_3) was chosen as the abrasive particle [granularity of 150–250 μm, polygonal prismatic, HV = 2000–2300 kg·mm^{-2}, figure 5(b)]. The airflow rate was regulated by controlling the inlet pressure valve, and the erosion angle was controlled by the home-made angle regulation support of erosion clamp. Erosion parameters were introduced as follows: erosion surface size = Φ17.5 mm; inner diameter of nozzle = 6 mm; distance from nozzle to specimens =150 mm; air pressure = 0.6 MPa; erosion angle =30°, 60°, and 90°; and erosion time = 30 + 30 + 60 + 60 + 60 s. Specimens before and after the erosion were cleaned by acetone ultrasonic waves. After being dried, the weight loss of specimens were weighted by a FA1004 analytical balance with a weight sensitivity of 10^{-4} g (all results were mean values of three specimens).

The thermal shock resistance of ceramic coating was tested in accordance with China Aviation Industry Standard HB7269-96. In the thermal shock test, specimens were heated by a SX2-4-9 chamber electric furnace to 850 °C, which was then kept for 15 min. Later, the specimens were taken out quickly and then cooled by tap water under room temperature. After being dried in a drying oven, the specimen surfaces were observed, and pictures were taken. This process was repeated until the specimens failed. If more than 30% of coating surface was peeled off, the specimen was considered as failure.

3. Results and discussions

3.1. Microstructure

3.1.1. Microstructure of plasma spraying coating

The surface morphology of plasma spraying AT13 coating is shown in figure 6. Figure 6(a) shows that the coating surface was uneven and stacked together in lamellar structures. The lamellar structure was formed immediately

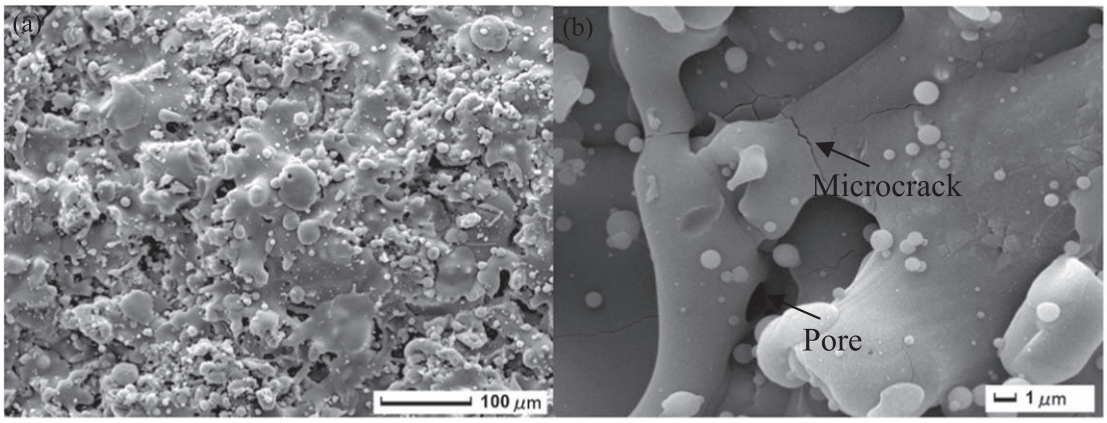


Figure 6. Surface morphology of plasma spraying AT13 coating surface: (a) low amplification, and (b) high amplification.

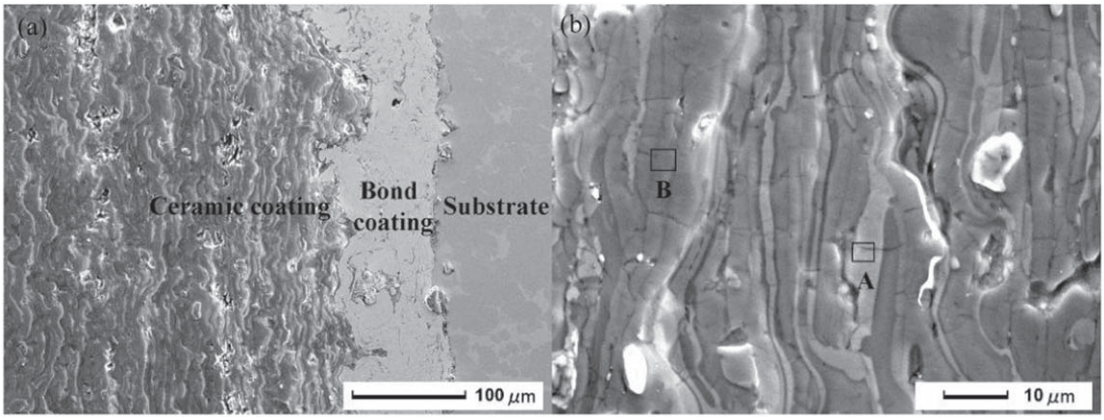


Figure 7. Cross-sectional morphology of the plasma spraying AT13 coating: (a) low amplification, and (b) local amplification of ceramic layer.

after solidification of sheet, which was paved on the formed coating surface when melted or semi-melted AT13 particles impacted onto the coating surface during plasma spraying. A small-sized bonding was present between lamellas, accompanied with many pores and low compactness. The high-amplification morphology in figure 6(a) is shown in figure 6(b). Pores, microcracks, and other defects could be clearly seen in the coating. Given that the sprayed particles overlap and stack mutually, gases in the melted particles precipitated as a response to volume shrinkage and the spraying of melted particles after the coating was cooled to room temperature, thus forming pores.

The cross-sectional morphology of plasma spraying AT13 coating is shown in figure 7. The AT13 composite ceramic layer, KF-113A transition layer, and TiAl alloy base are shown from the left to the right in figure 7(a). The AT13 ceramic coating has obvious lamellar stacking characteristics, which are determined by the technological characteristics of plasma spraying. Plasma spraying refers to heating of plasma heat source materials into the melting or thermoplastic state, thus forming a cluster of high-speed melted particle flow (molten droplet flow). This cluster of high-speed melted particles impacted onto the base or the formed coating surface successively. Through transverse flow flattening of particles, the melted droplets are solidified, cooled quickly, and then deposited continuously, thus forming the coating [9]. Due to considerably high flattening speed, cooling, and solidification speed in the process of coating formation by melted droplets, the melted droplets are independent under usual spraying conditions. One layer of spraying powder overlapped onto the previous coating continuously. Thus, the plasma spraying AT13 coating showed lamellar structures. Moreover, good mechanical bonding interfaces were formed between the AT13 ceramic layer and the KF-113A transition layer, as well as the KF-113A transition layer and the base. The ceramic structure is further amplified in figure 7(b) and the lamellar structural characteristics are more explicit. The coating presents obvious deep-shallow alternative lamellar structures.

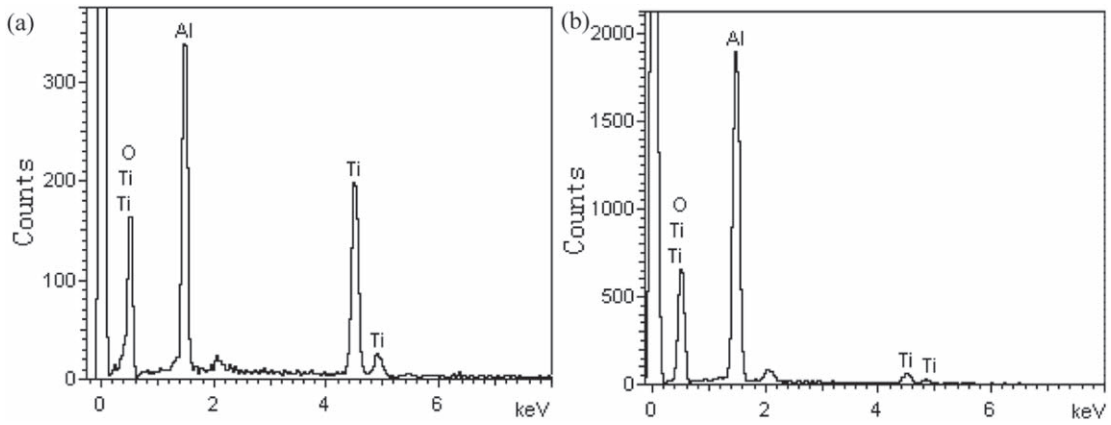


Figure 8. EDS results of AT13 coating: (A) zone A, and (b) zone B.

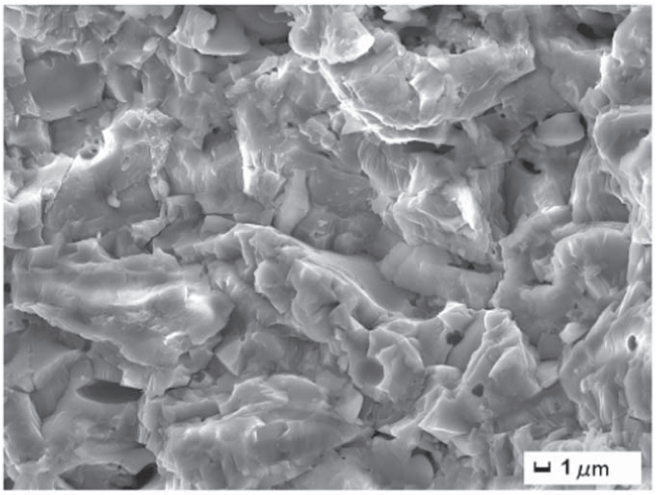


Figure 9. Sectional morphology of plasma spraying AT13 coating.

The EDS results of the light lamellar zone A and the deep lamellar zone B in figure 7(b) are shown in figure 8. The light structure is the zone rich of TiO_2, and the deep structure is the zone rich of Al_2O_3. Mutually diffused components were found between these two zones. This finding could be explained as follows. As the temperature was very high in the spraying process and the melting point of TiO_2 was lower than that of Al_2O_3, the TiO_2 powder melted and it could bond several Al_2O_3 together. The melted TiO_2 and Al_2O_3 formed mutual melting to some extent. Adding TiO_2 could lower porosity and increase the compactness of the coating; it is also conducive to increasing the bonding strength between the coating and the transition layer or the base material and to the adhesive aggregation intensity of Al_2O_3 in the coating, thus improving the mechanical properties of the coating. Therefore, Al_2O_3 coating with a certain proportion of TiO_2 has better toughness and higher impact resistance than pure Al_2O_3 coating.

The sectional morphology of the plasma spraying AT13 coating is shown in figure 9. In plasma spraying coating, a typical lamellar structure was obvious in the plasma spraying state, and it was formed by staggering and stacking of innumerable deformed particles in a fluctuating manner. Some pores or holes and microcracks could be observed between lamellas rather than forming tight bonding.

3.1.2. Microstructure of laser remelting ceramic coating

During preparation of ceramic coating based on the combination of laser remelting and plasma spraying, very high heating and cooling speeds, a great gap in the coefficients of thermal expansion between the ceramic coating and metal base, and volume shrinkage of the coating due to abundant gas escaping are present. Therefore, the laser remelting ceramic layer is easy to be cracked and peeled off. Thus far, many methods have been applied to decrease or eliminate cracks in the remelting layer, mainly including optimizing technical parameters, adjusting

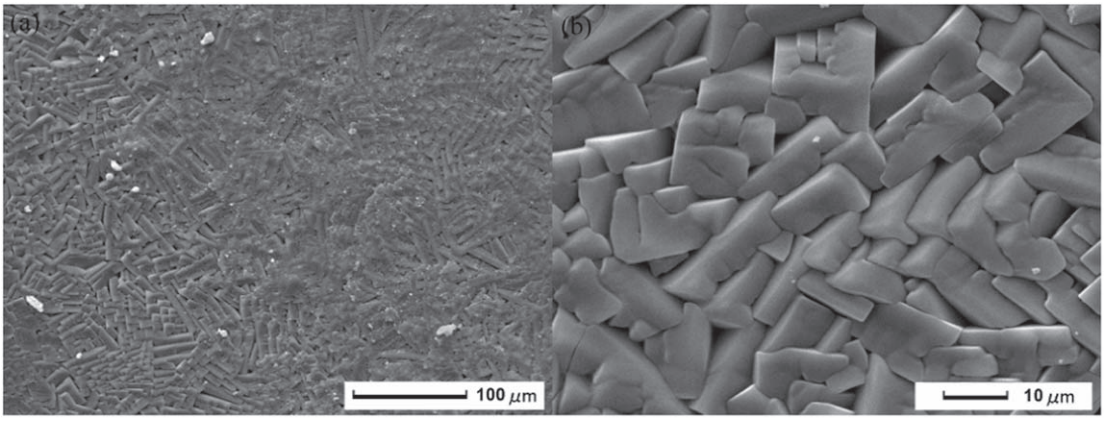


Figure 10. Surface morphology of the laser remelting AT13 coating: (a) low amplification, and (b) high amplification.

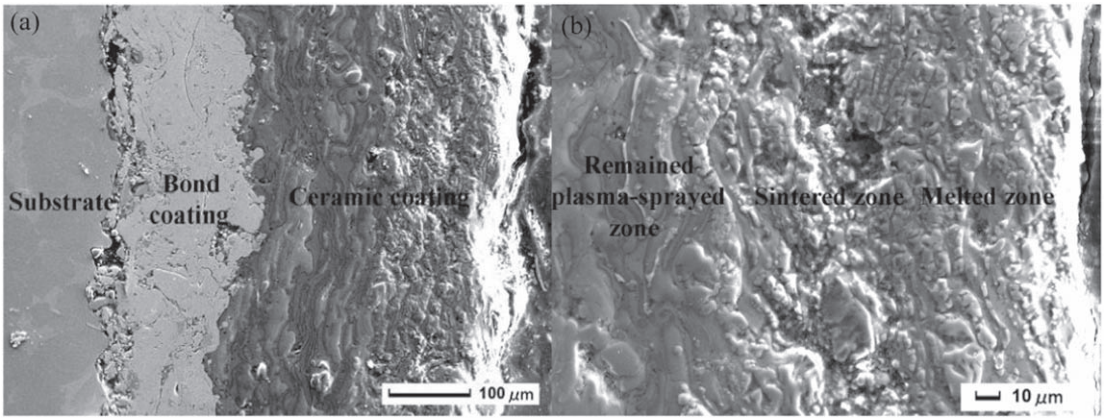


Figure 11. Cross-sectional morphology of the laser remelting AT13 coating: (a) low amplification, and (b) local amplification of ceramic layer.

composition of the coating materials, and introducing ultrasonic vibration into the remelting process. From the technological perspective, preheating of the base before laser remelting and slow cooling of the base after are effective measures to avoid cracks on the remelting layer. Similarly, using appropriate laser power could acquire a relatively good remelting layer. Considering the high power and great melting depth during laser remelting, the stress produced by volume shrinkage is also great at melting and cooling; this stress could not be relaxed effectively, thus making it easy to generate cracks. If the melting depth is small, that is, the melting layer is thin, the stress produced by volume shrinkage could be relaxed by pores below the remelting layer [53]. The test in the present study assured that only the ceramic coating surface was remelted by controlling the laser energy density, thus realizing the goal of controlling cracks on the remelting layer. The surface morphology of laser remelting AT13 ceramic coating is shown in figure 10. After laser remelting, the original plasma coating was remelted and crystalized, which caused significant changes in the phase structure and structures of the coating and thus forming small dense crystal structures. The laser remelting AT13 coating surface was more compacted and had better surface evenness than the plasma spraying layer. Moreover, the remelting surface basically had no defects, such as cracks.

The cross-sectional morphology of the laser remelting ceramic coating is shown in figure 11. The AT13 ceramic layer, KF-113A transition layer, and TiAl alloy base are shown from the right to the left in figure 11(a). Due to the comprehensive influences by laser power, energy density, temperature field distribution in the laser acting zone, AT13 ceramic thermal conductivity, and coating thickness, making the whole ceramic layer remelted during laser remelting was impossible. The remelted AT13 ceramic layer presented obvious hierarchical structural characteristics. In accordance with structural forms, the remelted AT13 ceramic layer could generally be divided into remelting zone, sintering zone, and residual plasma spraying zone [55]. The corresponding structure is shown in figure 12.

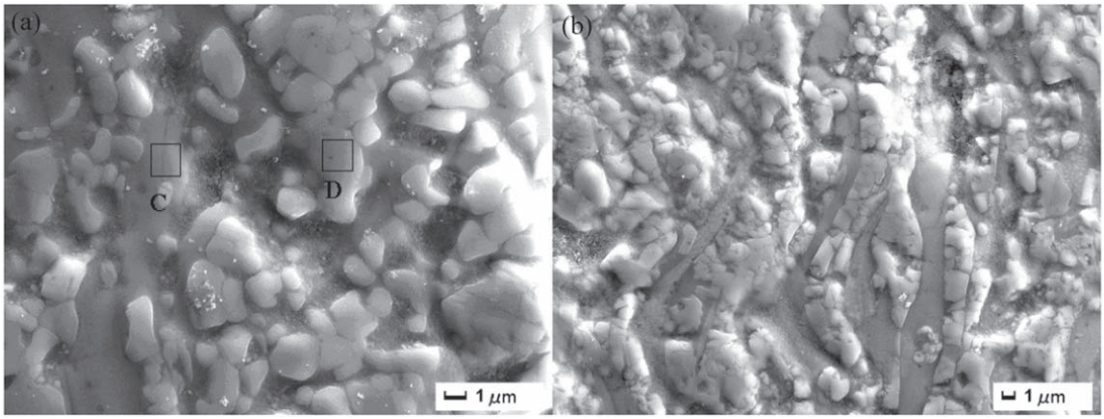


Figure 12. Morphology after laser remelting: (a) remelting zone, and (b) sintering zone.

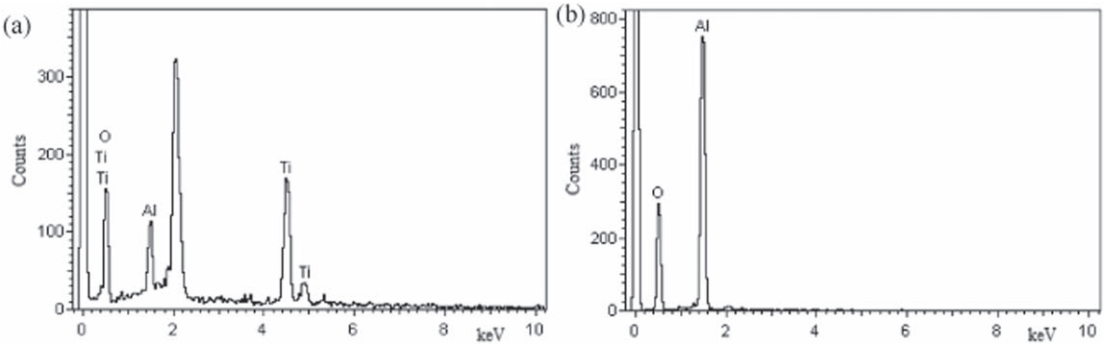


Figure 13. EDS results of laser remelting AT13 coating: (A) zone C, and (b) zone D.

The EDS results of the zone C and the zone D in figure 12(a) are shown in figure 13. The elements in zone C contain Al, Ti and O, while there are only Al and O elements in zone D, which is different from plasma-sprayed AT13 coating. Under the irradiation of laser high energy density, the molten pool temperature is very high, and the as-sprayed Al_2O_3 and TiO_2 melt at the same time. With the movement of laser, the molten pool temperature decreases, and most high melting point Al_2O_3 (2045 ^oC) solidifies first to form grains like zone D. With the further reduction of molten pool temperature, the remaining Al_2O_3 and low melting point TiO_2 (1840 ^oC) formed Al_2TiO_5 solid solution, which around first melted Al_2O_3 grains, as shown in zone C.

During laser remelting, the surface ceramic layer is melted by the high temperature, which is produced instantly, forming a high-temperature molten pool. In the follow-up solidification process, the thermal conductivity of ceramic layer is relatively low, the cold base could cool the ceramic layer slightly, and the heat loss of molten pool is mainly attributed to the thermal radiation and heat convection to the atmosphere. However, Ar gas protection was applied during remelting, the molten pool was cooled quickly. Due to the excessive degree of supercooling, small-sized isometric crystals were formed in the remelting zone, different from the columnar crystal structures, which are formed by the slow cooling of the molten pool and grow along the heat flux [55]. Due to heat conduction of the remelting zone, the temperature of the layer below the remelting zone reached the sintering temperature of AT13 ceramic. In the sintering process, driven by surface energy reduction, materials fill in neck and pores among particles through different diffusion methods, thus making the neck grow gradually. Meanwhile, small particles are bonded mutually and grains grow, while pores and crystal boundaries decrease gradually. The compactness of coating also increases. Eventually, the sintering zone is formed. In the ceramic layer near the transition layer, it is difficult for the heats from the remelting zone to be transmitted to the ceramic material due to the low thermal conductivity and the temperature of the ceramic material is relatively low. Finally, the ceramic layer maintains the original typical lamellar structural characteristics in the plasma spraying state [55].

The sectional morphology of the remelting layer of laser remelting AT13 coating is shown in figure 14. After laser remelting, most defects in the original plasma spraying layer were eliminated, and a remelting zone with dense, uniform, and small isometric crystals was formed on the coating surface.

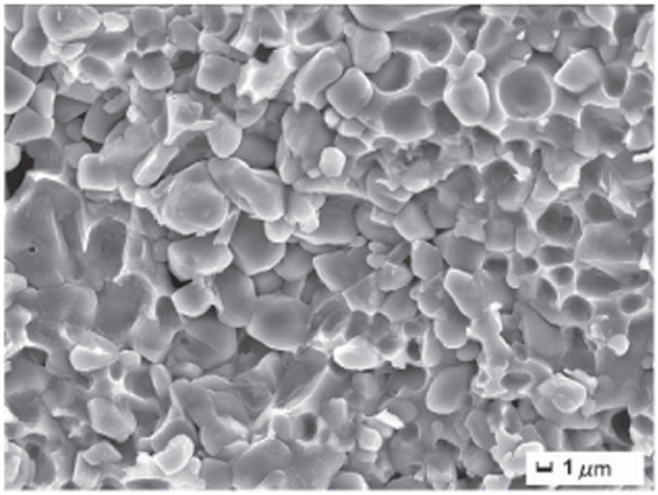


Figure 14. Sectional morphology of the remelting layer of laser remelting AT13 coating.

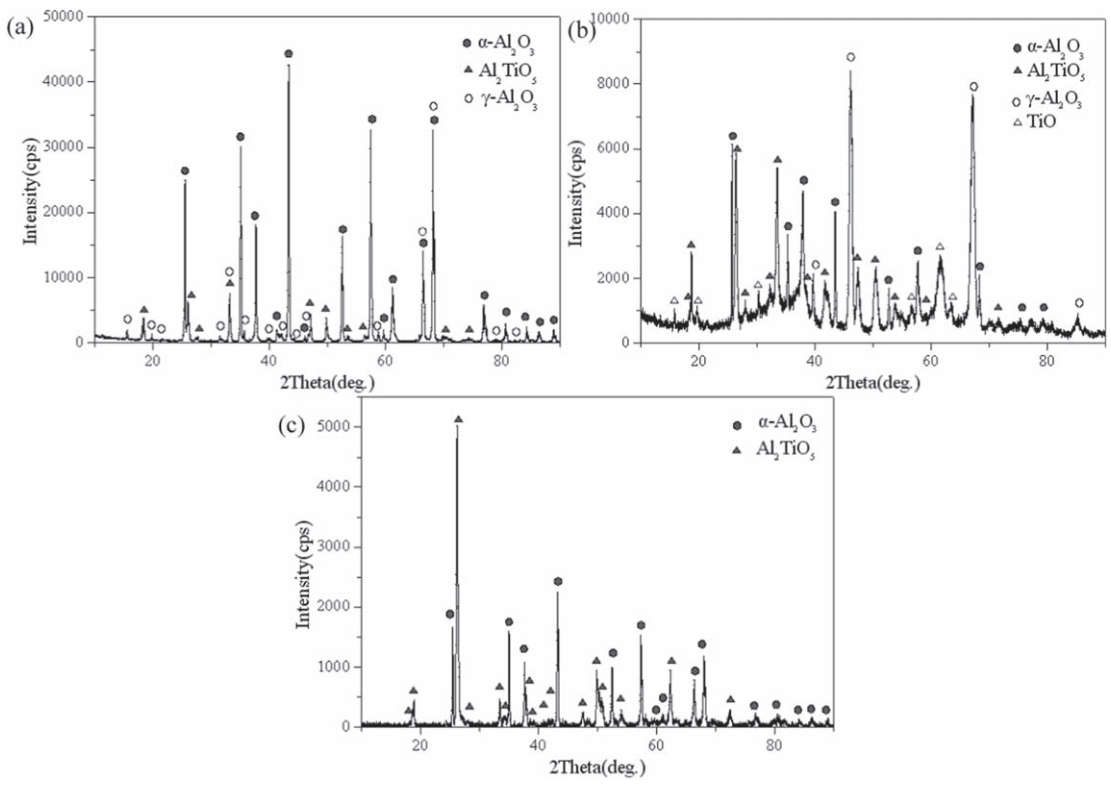


Figure 15. XRD spectra: (a) original AT13 powder, (b) plasma spraying AT13 coating, and (c) laser remelting AT13 coating.

3.1.3. Phase composition analysis of the coating

The surface XRD spectra of AT13 powder, plasma spraying AT13 coating, and laser remelting AT13 coating are shown in figure 15. The AT13 powder mainly existed in the form of steady α-$A1_2O_3$ and Al_2TiO_5 solid solution, accompanied with few metastable-phase γ-$A1_2O_3$. The plasma spraying AT13 ceramic coating was mainly composed of γ-$A1_2O_3$, α-$A1_2O_3$, and Al_2TiO_5. Besides, some TiO_2 was reduced to TiO in the plasma flame. Among these phases, a high content of γ-$A1_2O_3$ was found in the coating. Compared with the original powder, some α-$A1_2O_3$ transformed into γ-$A1_2O_3$ due to plasma spraying. The reason is because in the process of plasma spraying, the cooling speed of coating could reach as high as 10^6 °C–10^8 °C s^{-1}, and it is a typical fast solidification process, thus enabling the formation of metastable phase in the coating. The formation of metastable phase is not only closely related to the physical, chemical, and thermal properties of base material and

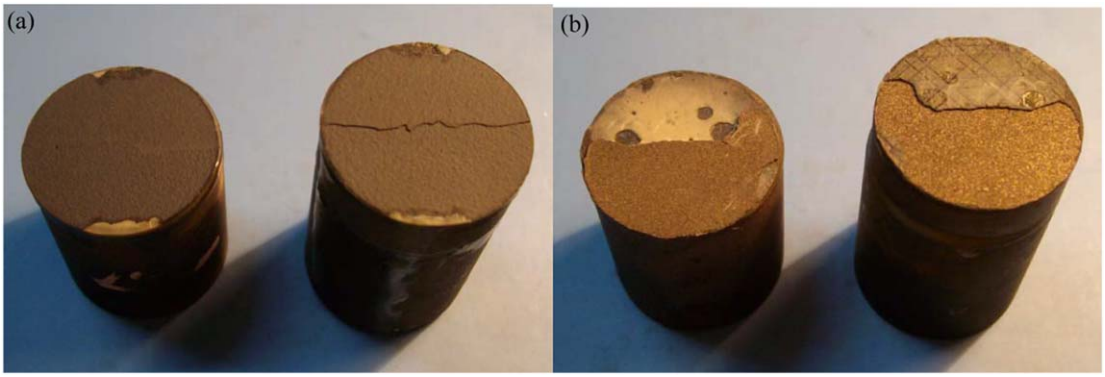


Figure 16. Separation morphology of specimens for bonding strength test of the coating: (a) plasma spraying AT13 coating, and (b) laser remelting AT13 coating.

Table 2. Bonding strength test results of specimens.

Coating type		Plasma spraying AT13 coating	Laser remelting AT13 coating
Tensile force/	Specimen 1	10.3 kN	25.7 kN
	Specimen 2	8.8 kN	22.6 kN
	Specimen 3	9.7 kN	28.5 kN
Average tensile force	9.6 kN	25.6 kN	
Average bonding strength	19.6 MP	52.1 MP	

ceramics but also to the melting degree, temperature jetting speed, and the distribution of ceramic particles and the temperature of base material. In the fast solidification process, the particles in the melt are in supercooled state. Under this circumstance, the condition of homogeneous nucleation is met. The nucleation capacities of different phases in the melt are determined by the critical nucleation free energy of solid phases rather than the free energies of different phases. Therefore, the phases with relatively lower critical nucleation free energy rather than those with low free energies form nucleation first. Given that γ-$A1_2O_3$ has a relatively low critical nucleation free energy during plasma spraying, it is easy to form nucleation. The nucleation rate of α-$A1_2O_3$ phase is relatively low. Therefore, γ-$A1_2O_3$ is the dominant metastable phase in the coating.

After laser remelting, γ-$A1_2O_3$ disappeared completely. Only α-$A1_2O_3$ and Al_2TiO_5 were present in the coating. Under the effect of laser, the metastable γ-$A1_2O_3$ phases all transformed into steady α-$A1_2O_3$ phases [44]. This finding could be explained as follows. During laser remelting, a high-temperature molten pool is formed on the AT13 ceramic coating surface by the high temperature produced instantly when the laser beams are radiated onto the surface. When the temperature is higher than 1200 °C, γ-$A1_2O_3$ is irreversibly transformed into α-$A1_2O_3$. Therefore, the melt is solidified by the cooling speed phase again in the single α-$A1_2O_3$.

3.2. Bonding strength

3.2.1. Bonding strength test results

The bonding strength test results are listed in table 2. The average bonding strengths of plasma spraying AT13 coating and laser remelting AT13 coating were 19.6 and 52.1 MPa, respectively. In other words, the bonding strength of the laser remelting coating was 1.66 times higher than that of the plasma spraying coating.

3.2.2. Analysis of bonding strength results

The surface morphologies of plasma spraying and laser remelting AT13 coating specimens after separation of mating plates are shown in figure 16. The plasma spraying specimens were separated inside the ceramic coating [figure 16(a)]. Breakage boundaries ran through the center area of the coating, and the stresses concentrated in the center of the coating. Moreover, crack propagation deflected for the free of great barriers. These results demonstrated that the lamellar structures in the plasma spraying layer were not bonded tightly. With the increase in spraying thickness, the upper layer was the weakest bonding point in the coating system. Internal stresses concentrated in some zones of the coating.

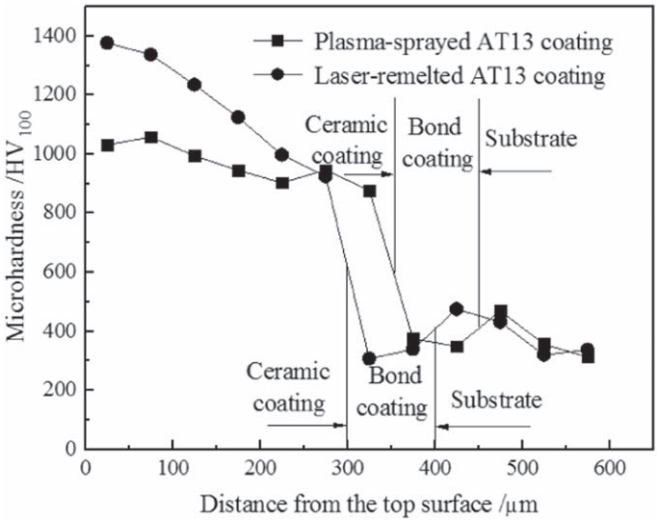


Figure 17. Microhardness distribution of cross section of specimens.

The separation morphologies of laser remelting coating specimens are shown in figure 16(b). The separation occurred between the bonding layer and the base. It was still through-wall crack expanding along the center area of the coating. The weakest position of the coating was transformed from the internal areas of the ceramic coating to the bonding layer and base. This finding revealed that laser remelting changed the internal structure of the coating effectively and the structure of the sintering zone (heat affected zone) became more compact. The bonding strengths among different layers improved significantly [48, 49]. Laser remelting could increase the bonding strength of the coating significantly because the stresses in the remelting and sintering layers were released, and the internal structure became more compacted.

3.3. Microhardness

Microhardness was measured at five points chosen randomly on specimen surfaces. The surface hardness of plasma spraying AT13 ceramic coating fluctuated greatly within 892.5–1207.6 HV_{100}, with an average hardness of 1045.0 HV_{100}. This finding is related to the nonuniformity, loose structure, and some pores in the coating. Due to these defects, the coating was crushed in the loading process. Moreover, measuring the indentation size was difficult, and the measurement accuracy was relatively low. Laser remelting AT13 ceramic coating showed higher hardness (1320.8–1597.3 HV_{100}), with an average of 1461.2 HV_{100}, approximately 40% higher than that of the original plasma spraying coating. Moreover, the hardness was relatively stable because a uniform, continuous, and compact AT13 composite ceramic coating was formed after laser remelting.

When testing the microhardness of the cross section of the coating, a point was created every 50 μm in a longitudinal directioNn and 50 μm in a transverse direction from surface to inside. The microhardness distribution curve of the cross section of specimens are shown in figure 17. The hardness of laser remelting AT13 ceramic coating obviously decreased gradually along the depth direction. The hardness of the ceramic zone near the transition layer is basically equal to that of the plasma spraying layer. This finding also agrees with the ceramic layer composed of remelting zone, sintering zone, and residual plasma spraying zone after laser remelting. Moreover, the microhardness of the base zone close to the coating was slightly higher than that of the original TiAl alloy regardless of whether it was plasma spraying coating or laser remelting coating. This finding may be related to the spraying processing before plasma spraying and the thermal effect during plasma spraying and laser remelting.

3.4. Frictional wear performances

3.4.1. Frictional wear test results

The wear loss curves of plasma spraying and laser remelting AT13 composite ceramic coatings are shown in figure 18. The wear losses of the plasma spraying layer and the laser remelting layer achieved approximately linear growths as the wearing time went on. However, the variation rate of the wear loss of the laser remelting layer was small as time went on, and the wear loss was only 1/2–1/3 of that of the plasma spraying layer. In other words, the wear resistance of the laser remelting layer was 2–3 times of the plasma spraying layer. The reason is because laser remelting eliminates the structural nonuniformity, loose structure, pores, and other defects of the

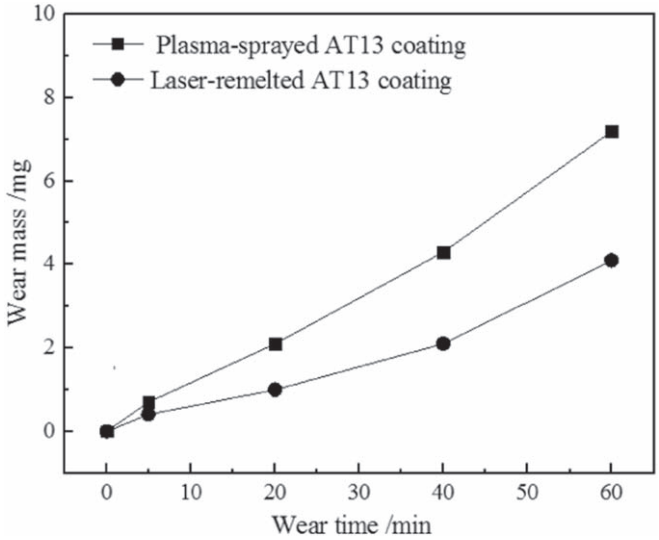


Figure 18. Variation curve of wear loss with time.

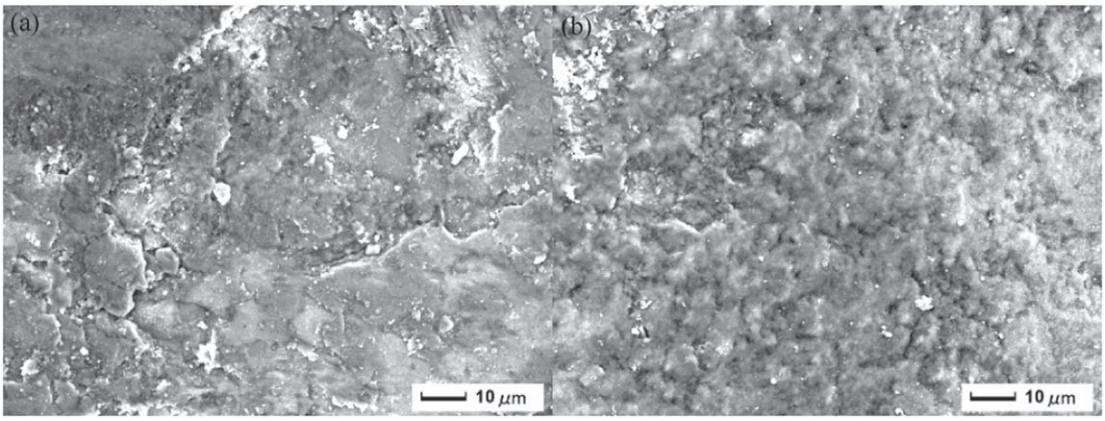


Figure 19. Wear morphology: (a) plasma spraying AT13 coating, and (b) laser remelting AT13 coating.

plasma spraying layer [40–47]. In addition, uniform, dense, and small isometric crystals are gained, thus increasing the hardness of the coating significantly. As a result, the wear resistance is extensively improved.

3.4.2. Frictional wearing mechanism analysis

The wear surface morphologies of plasma spraying and laser remelting AT13 coatings are shown in figure 19. Many microcracks and peeling pits were obviously seen on the wear surface of plasma spraying AT13 coating, because the particles in the plasma spraying ceramic coating mainly form mechanical bonding, which has low bonding strength and poor compactness of the coating. Therefore, cracks could be easily initiated on the particle interfaces under the effect of alternating stress, and then they propagate and connect mutually, finally making the particles peel off and developing peeling pits on local surfaces [53]. To sum up, fatigue-induced micro-peeling is the major wear mechanism of the AT13 plasma spraying layer, accompanied with wearing of the peeling layer.

The wear surface morphology of laser remelting AT13 coating is shown in figure 19(b). Comparison of the typical microscopic peeling morphologies showed that some microcracks were formed on the wear surface, but the quantity was significantly lower than that on the plasma spraying layer. This finding reflected that fatigue-induced microscopic peeling is still the major wearing mechanism of the laser remelting layer. The remelting layer showed higher compactness, more refined structure, and higher hardness and bonding strength than the plasma spraying layer. Therefore, it had fewer microcracks, a lower degree of microscopic peeling, and significantly higher wear resistance than the plasma spraying layer [53].

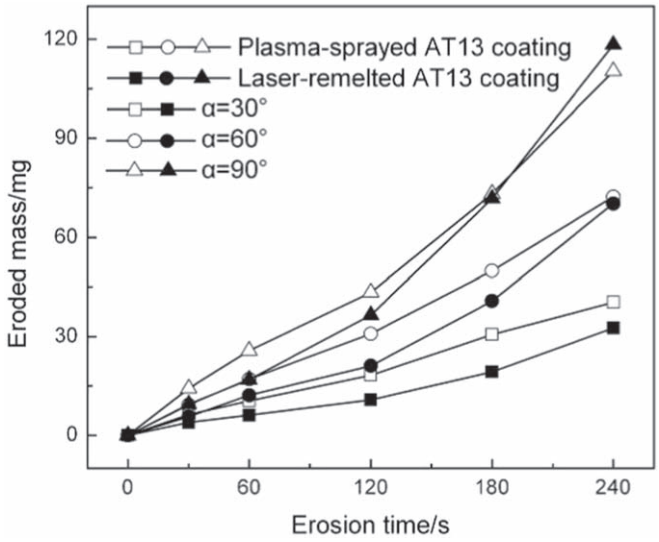


Figure 20. Erosion wear test results of AT13 coatings under different erosion angles.

3.5. Erosion property

3.5.1. Erosion behavior of coatings

The erosion test results of AT13 ceramic coatings under different erosion angles (30°, 60°, and 90°) are shown in figure 20. The curves showed that given the same conditions, the erosion-induced weight loss of the laser remelting specimens was lower than that of the corresponding plasma spraying specimens, indicating that laser remelting coating has better erosion resistance. For both layers, the erosion-induced weight loss increased linearly as time went on. However, the erosion-induced weight loss of the laser remelting specimens accelerated obviously when the erosion time was prolonged. Under the erosion angle of 90°, the laser remelting specimen showed the highest erosion-induced weight loss after 240 s. Moreover, the weight losses of both coatings were the lowest at 30° and reached the peak at 90°, manifested as erosion characteristics of typical brittle materials. The weight losses of plasma spraying AT13 coating at 30°, 60°, and 90° after 240 s were 40.4, 72.3, and 110.3 mg, respectively.

3.5.2. Erosion failure mechanism analysis of coatings

When abrasive particles impact onto the coating surface, the speed component could be decomposed into vertical speed component and horizontal speed component. The former mainly provides impact effect, while the later mainly provides cutting effect. For brittle AT13 ceramic coating, the horizontal speed component of the erosion particles was relatively high under low erosion angle. Due to the high hardness, the erosion-induced weight loss of brittle AT13 ceramic coating caused by cutting effect was relatively low. As abrasive particles have small vertical speed component and low energy, their impacts onto the coating were relatively small. As a result, brittle ceramic coating with high hardness had relatively strong erosion resistance under low erosion angles. Under high erosion angle, the abrasive particles with high vertical speed component impacted onto the coating surface strongly. Thus, brittle coating was easy to develop, and many cracks could easily propagate, finally resulting in the breakage and peeling of the coating. Therefore, brittle ceramic coating has poor erosion resistance under high erosion angles.

Surface SEM images of plasma spraying AT13 coating after erosion under 60° are shown in figure 21. The coating surface exhibited obvious peeling characteristics and micro fractures to some extent after erosion. Plasma spraying AT13 coating was formed by embedding and overlapping of lamellar particles, and the particles were mainly connected by mechanical riveting, resulting in low bonding force. The particle interfaces could be easily damaged. In the erosive wearing process, cracks propagate towards the bonding interfaces along the interlayer unbonded interfaces under the repeated impacts of abrasive particles; thus, the upper lamellar structures that bear the impacts directly peel off from the coating continuously [82, 83]. The corresponding erosion failure is shown in figure 22.

The erosion equipment used in this study was reconstructed from the sand-blasting machine. Compared with the ASTM-G76-83 standard (Standard Erosion Method of Solid Particles in Airflows), the abrasive particles were large, and the air pressure was relatively high, thus resulting in great erosion energies. Given the high-energy erosion (e.g., high erosion angle, big particles, and high speed), the impact energy of abrasive particles keeps the coating at the compression-tensile stress state continuously. Due to the low toughness and high

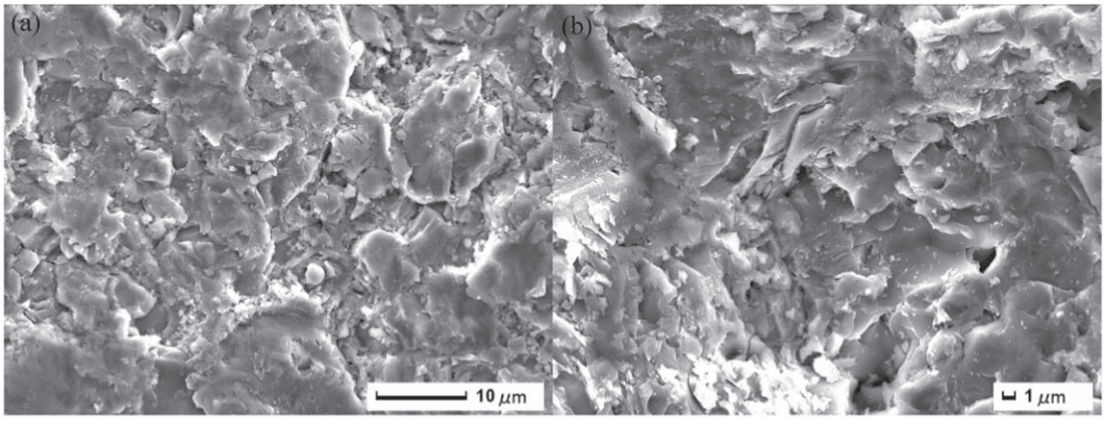


Figure 21. Typical morphologies of erosion surface of plasma spraying AT13 coating at 60°: (a) low amplification, and (b) high amplification.

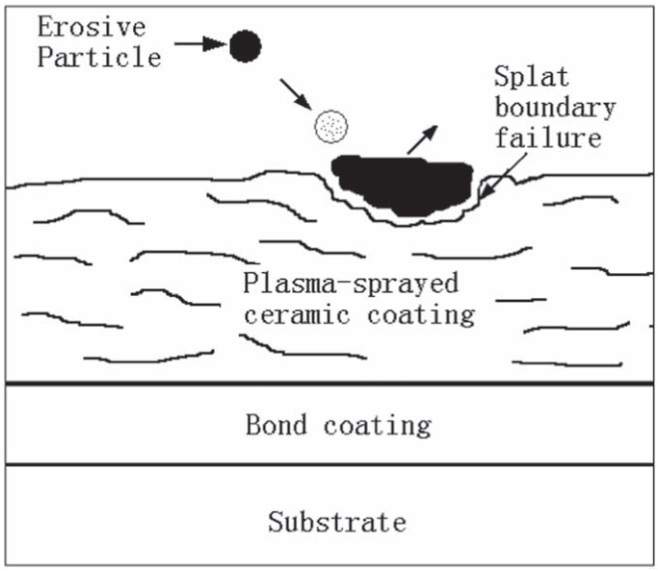


Figure 22. Erosive failures of plasma spraying AT13 coating.

brittleness, the AT13 ceramic could not consume erosion energies through plastic deformation. Under the alternative compression-tensile stresses, which are produced at the impacts of abrasive particles, the coating could be easily broken and separated from the matrix, thus losing weight. Therefore, the erosive wear of plasma spraying AT13 ceramic coating is dominated by lamellar peeling, accompanied with breakage of brittle ceramic particles to some extent.

Surface SEM images of laser remelting AT13 coating after erosion under 60° are shown in figure 23. Figure 23(a) shows that the laser remelting specimen had lighter peeling and fracture of erosion surface than the plasma spraying specimen, but relatively serious fractures were present in local areas [figure 23(b)]. After laser remelting, the plasma spraying ceramic coating became uneven. Remelting crystallization occurred on the porous loosen surface, lamellar structure disappeared, and a compact remelting layer was formed. Moreover, the surface was relatively even. Given the relatively high cohesion in the remelting layer, it was difficult to be peeled off during erosion. Instead, cracks initiated and propagated on near surface, finally resulting in breakage of the coating. Crystal peeling is the dominant failure mode. The principle of erosion failure is shown in figure 24.

Laser remelting specimen has high bonding strength and hardness in the initial stage of erosion. The compact remelting layer with few defects has strong resistance to crack initiation and propagation. It has smaller erosion-induced weight loss and good erosion resistance [84]. Moreover, the small roughness of laser remelting specimen could increase the erosion resistance to some extent, and the valid contact area exposed to abrasive particle beam decreases with the reduction in roughness. For plasma spraying specimen, the swelling zone is very

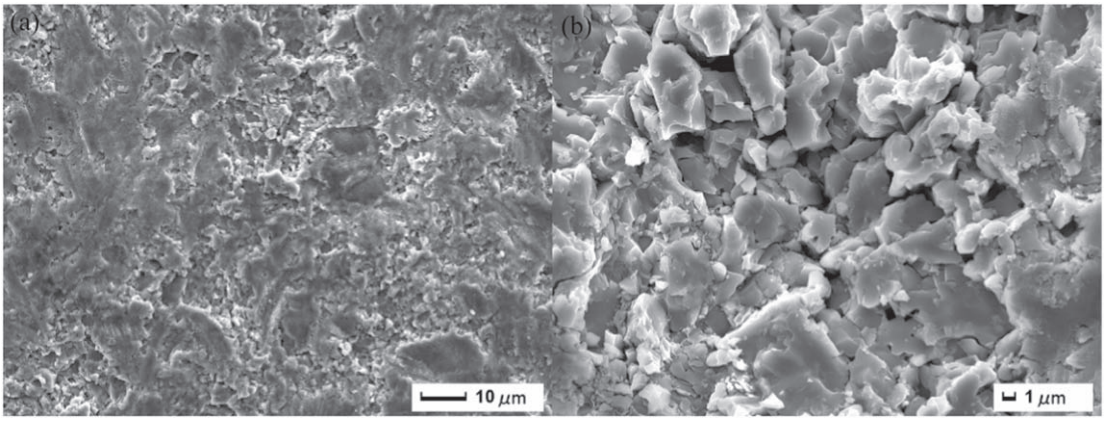


Figure 23 Typical morphologies of erosion surface of laser remelting AT13 coating under 60°: (a) low amplification, and (b) high amplification.

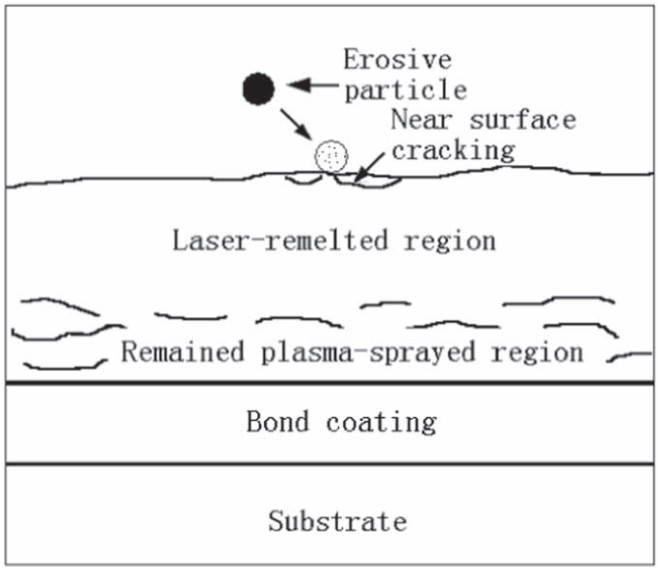


Figure 24. Erosion failure of laser remelting AT13 coating.

easy to be damaged by external particles due to the small constraint from the surface layer and the high probability of impacts by solid particles, resulting in the cracking of the coating and lamellar peeling. Therefore, the erosion rate of specimens increases. The erosion resistance of materials is improved with the reduction in surface roughness of the laser remelting specimen. However, due to poor shock resistance and low breaking tenacity, ceramic materials could easily develop cracks and pores and even peel off under dramatic heating and cooling conditions in the process of laser remelting, accompanied with great residual stresses [84]. Although laser remelting was performed to specimens under relatively optimal technological parameters in the experiment, defects such as cracks and pores could not be avoided completely, especially in the overlapping remelting zone. Due to the collaborative effects of the repeated impacts of abrasive particles and residual stress produced by thermal stress in laser remelting, the local regions with relatively more defects on the remelting surface could easily develop large and deep macrocracks, thus resulting in deep large-scaled peeling off at some positions. Some may even peel off to the interface between the remelting layer and the residual plasma spraying layer. This finding is different form the stepwise lamellar peeling mechanism of the plasma spraying layer under erosion. Therefore, the weight loss of laser remelting specimens accelerates under long-term erosion conditions.

The above analysis showed that laser remelting could improve the erosion resistance of plasma spraying ceramic coating to some extent. Due to cracks, residual stress, and other defects in the process of laser remelting, the erosion resistance was improved to a limited extent, especially under long-term erosion conditions. Therefore, the erosion resistance of laser remelting ceramic coating must be further improved, and measures

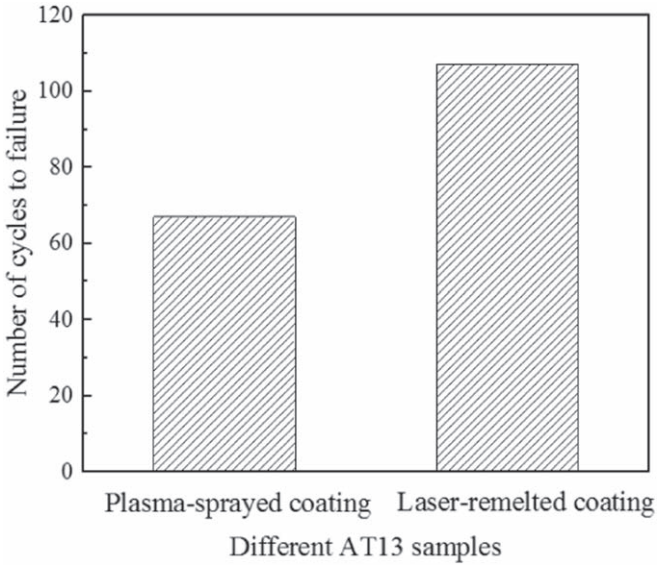


Figure 25. Number of thermal shock failures of different specimens.

must be adopted to decrease defects during the remelting process. Many measures, such as adding rare earth elements into the spraying powder, mixed spraying of ceramic powder and ceramic material with low melting point, controlling laser remelting parameters to form ordered phases in the ceramic layer, controlling and improving the quality and composition of the coating, and introducing ultrasonic vibration during laser remelting, could control cracks and peeling problems to some extent. In addition, nanomaterials have excellent properties beyond the reach of ordinary materials due to their unique structures. They provide beneficial conditions to improve coating performances. Laser remelting of nanostructured plasma spraying ceramic coating could obtain nanoparticle-reinforced coating, and the remelting layer has excellent tenacity due to the diffusion strengthening mechanism of nanoparticles, thus solving the easy cracking problem of laser remelting ceramic coating [19–21, 59, 62].

3.6. Thermal shock performances

3.6.1. Thermal shock test results

The comparative test results of the thermal shock performances of plasma spraying and laser remelting AT13 ceramic coatings under 850 °C water quenching are shown in figure 25. The plasma spraying and laser remelting coatings suffered from 67 and 107 thermal shock failures, respectively. This finding proved that laser remelting could improve the thermal shock performances of plasma spraying layer effectively.

Pictures of surface changes in the thermal shock process of plasma spraying AT13 specimens are shown in figure 26. The specimens obviously showed relatively good thermal shock resistance in early stage. After 43 thermal cycles, the coating surface developed neither macrocracks nor peeling phenomenon, and it was hardly damaged. It was until 44 thermal shocks that macrocrack was initiated at the corners of the coating. However, once the crack was formed, the coating began to peel off. With the increase in thermal shocks, cracks and the peeling zone propagated quickly on the coating surface. The peeling area of the coating surface reached 30% after 67 thermal shocks, and the coating failed.

Pictures of surface changes in laser remelting AT13 coating during thermal shocks are shown in figure 27. The failure mode clearly differed significantly from that of plasma spraying specimen. During thermal shock test, plasma spraying coating basically developed peeling at the corners, while laser remelting coating had peeling at the corners and local peeling in central areas. With the increase in thermal shocks, the peeling zone of laser remelting coating expanded slowly. Although the number of thermal shocks for peeling of two coatings was basically equal, the total thermal shock life of laser remelting coating was approximately 60% longer than that of plasma spraying coating.

3.6.2. Thermal shock failure mechanism analysis of coatings

Ceramic coatings could finally fail under repeated high-temperature thermal shocks. Coating failure is attributed to many reasons, among which internal stress produced during thermal shocks is the primary reason. The growth of thermally grown oxide (TGO) on the interface between the transition layer and the ceramic layer

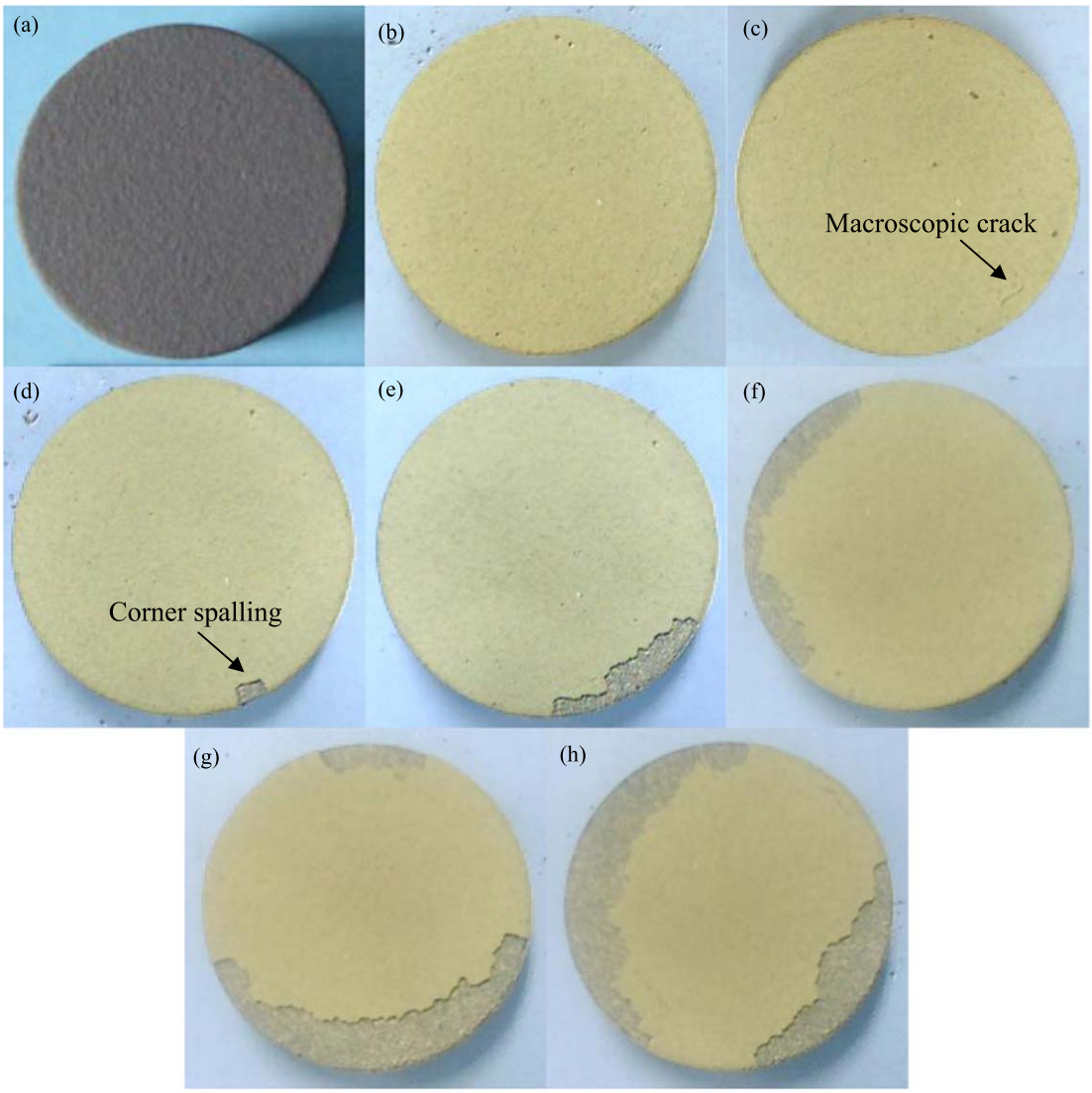


Figure 26. Pictures of surface changes in plasma spraying AT13 coating at different thermal shock cycles under 850 °C: (a) 0, (b) 43, (c) 44, (d) 45, (e) 51, (f) 61, (g) 65, and (h) 67.

during thermal shocks also influences the coating failure significantly. In addition, transformation stresses could assist thermal shock failure of coatings to some extent.

Thermal stress in coating is formed in the high-temperature thermal cycles of coatings because of the temperature difference between the coating and the base material, and the differences in expansion coefficient between the ceramic coating and the transition metal bottom and between the transition layer and the base. In a thermal cycle, the volume changes in the ceramic surface layer and the metal base or metal bottom differ because of their different thermal coefficients of expansion, thus resulting in different stress states of the coating surface during temperature rising and reduction. In the stage of temperature rising, compressive stress is produced in the surface ceramic layer. In the cooling process, tensile stress is produced on the surface layer, as shown in figure 28(a). In the repeated thermal shocks, a residual tensile stress layer is formed on the coating surface. This residual tensile stress layer may make the coating bend [figure 28(b)]. Influenced by this bending force, stresses concentrate on the coating surface and the coating-transition layer interface. When the tensile stress exceeds the breaking strength of coatings, the coating surface is fractured, that is, it generates longitudinally distributed cracks, as shown in figure 28(c). When the interface stress exceeds the bonding strength of interfaces, cracks parallel to the coating are formed, thus resulting in the peeling off of the ceramic surface layer.

During thermal shocks of ceramic coating, longitudinal and horizontal cracks at the bonding layer differently influences the thermal shock life of coatings. On the one hand, longitudinal cracks on the surface bring oxygen from air into the coating and make it diffuse towards the bonding layer, thus causing oxidization of the transition layer and forming the TGO layer. This TGO layer causes horizontal cracks at the bonding layer directly, thus influencing the thermal shock performances of the coating. On the other hand, the production of

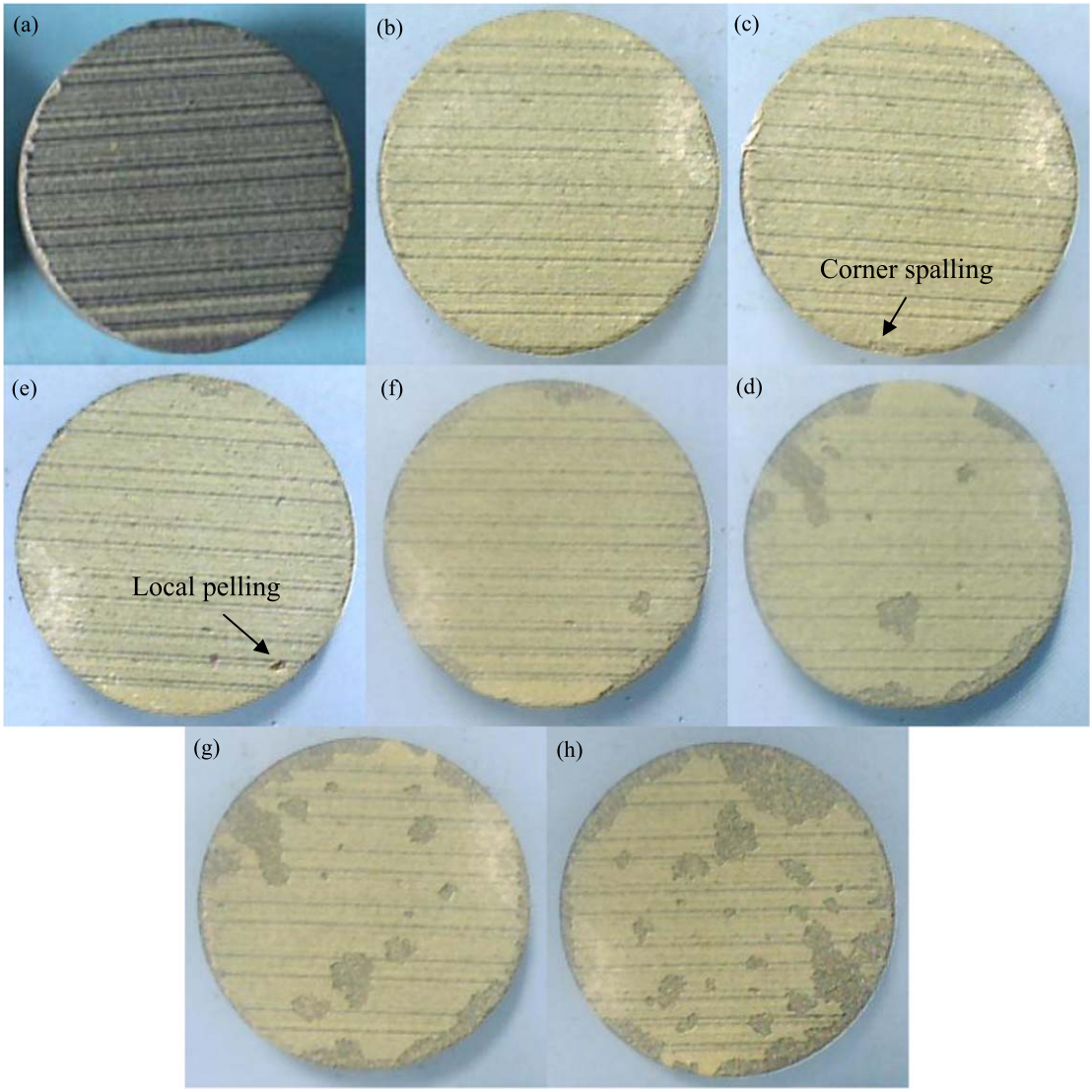


Figure 27. Pictures of surface changes in laser remelting AT13 coating at different thermal shock cycles under 850 °C: (a) 0, (b) 30, (c) 31, (d) 36, (e) 67, (f) 80, (g) 92, and (h) 107.

longitudinal cracks not only could effectively relieve thermal stress in thermal cycles and lower the propagation force of horizontal cracks but also improve the thermal shock resistance of coatings. Once horizontal cracks initiate, the bonding layer may propagate along the bonding layer during thermal shocks, finally making the coating peeled off and shortening the thermal shock life of coatings.

Surface microstructures of plasma spraying AT13 coating before and after thermal shocks under 850 °C are shown in figure 29. Compared with figures 29(a), (b) (unpeeled zone) shows obvious networked cracks on the coating surface. The thermal shock resistance of coatings was determined by the bearing capacity of thermal stress and strength of the coatings (including the bonding strength of coating and transition layer/matrix and cohesive strength of the coating) under thermal shocks. The positions in plasma spraying AT13 ceramic coating had pores, and weakly bonded lamellar structures were easy to form crack sources under thermal cycling stresses. Moreover, the coatings lacked an effective mechanism to relieve thermal stresses. Thus, cracks could easily form during thermal cracks, especially horizontal cracks on the bonding layer. Given the repeated actions of thermal stresses, horizontal cracks propagated quickly and the coating was peeled off accordingly, manifested by poor thermal shock performances [86–88]. One study [47] has pointed out that plasma spraying coating has poorer high-temperature oxidization resistance, quicker growth of TGO on the interface between ceramic layer and transition layer during high-temperature oxidization, and higher growth rate of TGO on the plasma spraying AT13 coating interface during thermal shocks than laser remelting coating. Although the TGO membrane is vital to prevent further oxidization of the transition layer and to protect the matrix, excessively thick TGO may weaken the bonding force of the transition layer, thus accelerating the peeling off of the coating.

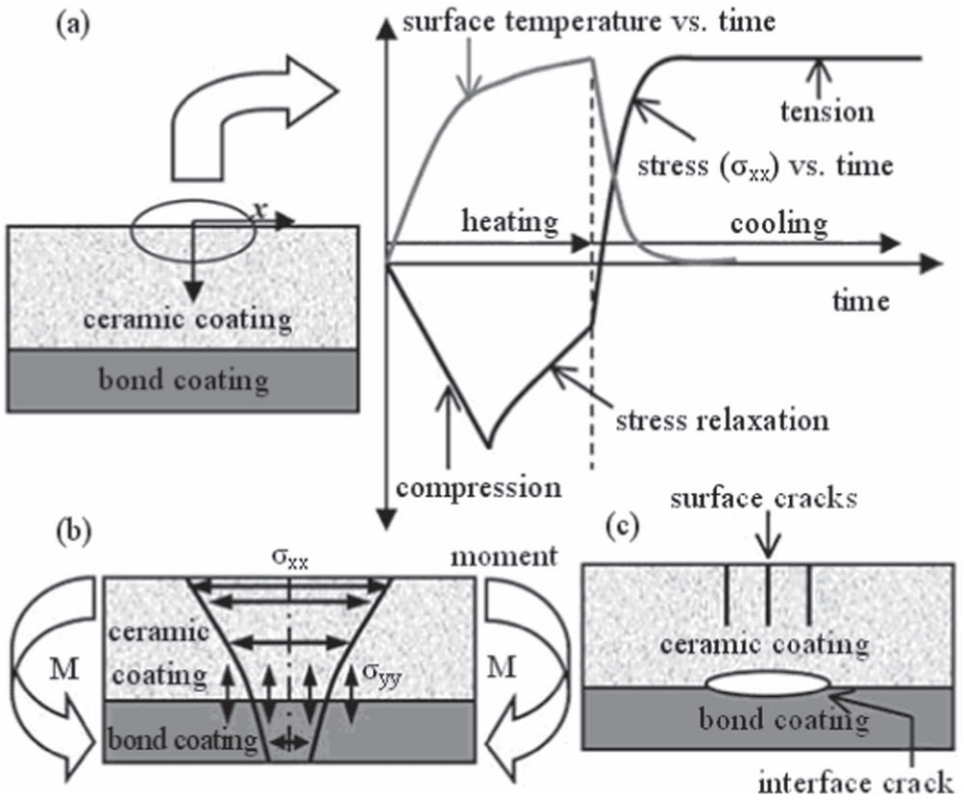


Figure 28. Production of stresses, surface cracks, and horizontal cracks on ceramic coatings during thermal shocks: (a) temperature-stress relations during thermal shocks, (b) residual stress produced during thermal shocks, and (c) crack initiation during thermal shocks. Reprinted from [85], Copyright (2004), with permission from Elsevier.

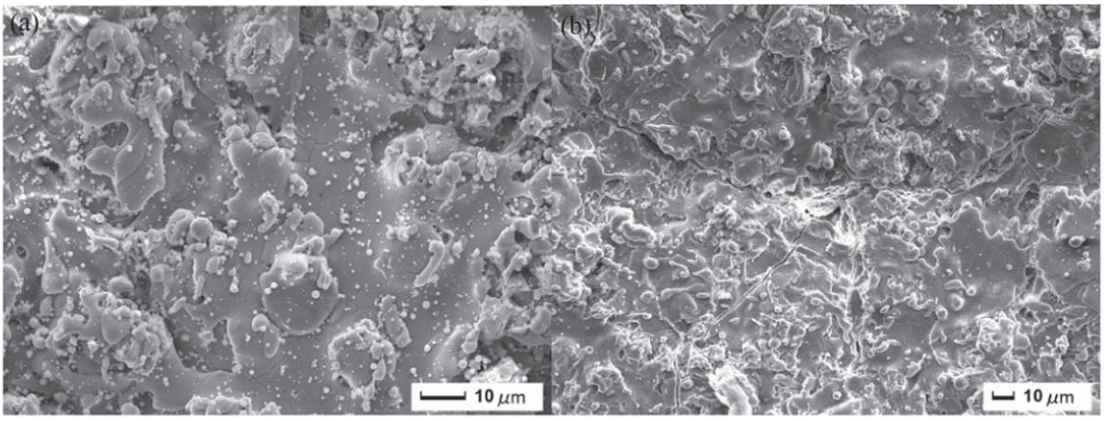


Figure 29. SEM images of plasma spraying AT13 coating surface: (a) before thermal shocks, and (b) after 67 thermal shocks.

According to the thermal shock test results, a large area of ceramic coating peeled off from the bonding layer and then failed after several (67) thermal shocks of plasma spraying AT13 coating.

Typical morphologies of laser remelting AT13 coating before and after thermal shocks are shown in figure 30. The microstructure of the unpeeled surface after 107 thermal shocks is shown in figure 30(b). Compared with the surface morphology of plasma spraying AT13 coating after thermal shocks, it presented a similar crack network, but the density was higher and crack size was smaller, belonging to microcracks. Longitudinal cracks on the surface are conducive to relieve thermal stress during thermal shocks. In particular, microcracks have been proven as stress releasing source. Microcracks could improve the tenacity of materials significantly and greatly relieve thermal stress during thermal shocks, thus improving the thermal shock resistance of materials. Moreover, dense isometric crystals were formed after laser remelting, while the pores and

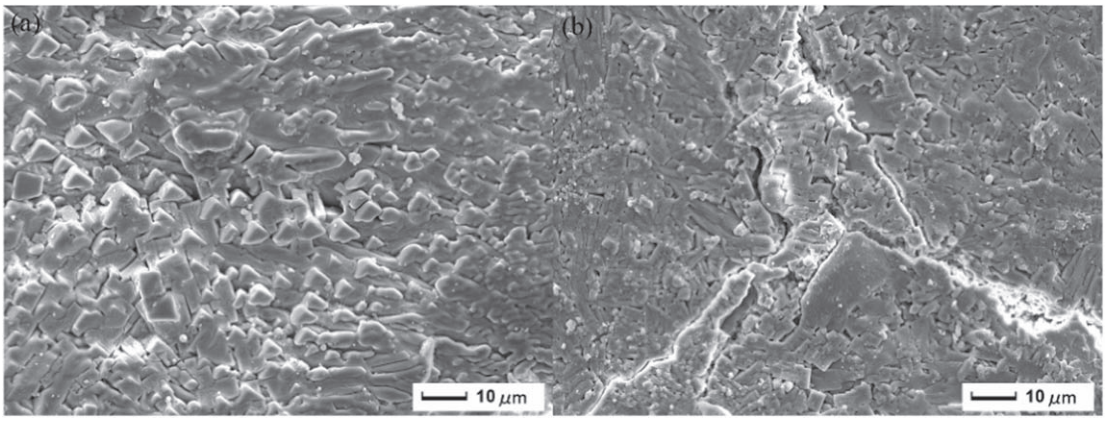


Figure 30. SEM morphologies of laser remelting AT13 coating surface: (a) before thermal shocks, and (b) after 107 thermal shocks.

lamellar structures in plasma spraying coating decreased. These findings changed the pathway for direct diffusion of oxygen in the ceramic layer as lamellar interface or defects, such as pores. Although networked microcracks initiated during thermal shocks, thermal expansion could make cracks closed effectively during heating and insulation, thus hindering direct diffusion paths of oxygen. The overall oxidation resistance of coating improved accordingly. Therefore, TGO grew slowly on the laser remelting AT13 coating during thermal shocks, and the thermal shock resistance of the coating improved. Nevertheless, cracks and pores could be easily produced and even peeling problems of ceramic materials, upon extensive heating and cooling during laser remelting. This finding is attributed to the poor shock resistance and low breaking tenacity, accompanied with great residual stress. Cracks, pores, and other defects could not be completely avoided during laser remelting even though relatively optimal technical parameters were applied in the experiment, especially in the overlapping remelting zone. Therefore, many defects could be found during thermal shocks, and the regions with great residual stress were easy to have crack propagation, thus making laser remelting samples easy to develop local unit dotted peeling. The peeling generally occurs between the laser remelting layer and the residual plasma spraying layer. With the increase in thermal shocks, the peeling units increased, and some peeling units connected mutually into large-scaled peeling. However, most regions with few defects still showed good thermal shock resistance. Therefore, although the number of thermal shocks for peeling off of the laser remelting coating was basically equivalent to that of the plasma spraying coating, the total number of failures increased significantly.

Based on the above comparative analysis, laser remelting coating could more easily develop local unit dotted peeling during thermal shocks than plasma spraying coating, and this finding is related to some defects produced in the remelting process. In other words, laser remelting lowers the initial resistance to thermal shocks in the local areas of the ceramic coating, but the total thermal shock resistance of laser remelting coating is significantly better than that of the plasma spraying coating. Defects, such as cracks and pores, produced during laser remelting could be further decreased if the measures in section 3.5, including adding rare earth elements into spraying powder, changing the laser output mode, introducing in ultrasonic vibration, and preparing nanostructured coating, are adopted. In this manner, laser remelting could improve the thermal shock performances of plasma spraying coating significantly.

4. Conclusions

Al_2O_3-13 wt% TiO_2 composite ceramic coating was prepared on the TiAl alloy by using plasma spraying, and the coating was processed by laser remelting. The influences of laser remelting on the microstructure, bonding strength, microhardness, wear resistance, erosion resistance, and thermal shock resistance of the coating were studied systematically.

(1) The plasma spraying AT13/KF-113A composite coating forms well mechanical bonding with the base. However, the AT13 composite ceramic coating has typical lamellar structures and low compactness. α-$A1_2O_3$ is transformed partially into γ-$A1_2O_3$ after plasma spraying. Given the relatively optimal technological parameters, the particles on the surface ceramic coating are refined, lamellar structures disappear, and compactness is increased after laser remelting. Defects, such as crack, are hardly noticed on the remelting layer. The metastable-phase α-$A1_2O_3$ is transformed partially into stable-phase α-$A1_2O_3$ after

laser remelting. The whole remelted ceramic coating forms a remelting zone with fine isometric crystals, a sintering zone, and a lamellar residual plasma spraying zone.

(2) The bonding strength, microhardness, wear resistance, erosion resistance and thermal shock performances of plasma spraying AT13 ceramic coating could be improved significantly after laser remelting.

(3) Microscopic peeling caused by brittle fatigue is the major wearing mechanism of plasma spraying AT13 ceramic coating, accompanied with a certain degree of peel wearing. Microscopic peeling caused by brittle fatigue is also the major wearing mechanism of laser remelting AT13 ceramic coating.

(4) Plasma spraying and laser remelting AT13 ceramic coatings present typical brittle erosion characteristics. The erosive wearing of the plasma spraying coating is dominated by lamellar peeling off, accompanied with brittle ceramic particle breakage to some extent. The erosive wearing of the laser remelting coating is mainly dominated by near-surface crack initiation and propagation, finally resulting in the fracture of the remelting layer and grain peeling.

(5) Although laser remelting decreases the initial thermal shock resistances of the local areas of the ceramic coating, the laser remelting coating has relatively longer service life against thermal shocks than the plasma spraying coating. With respect to thermal shock-induced failure mode, the plasma spraying coating is basically peeled off at the corners, while laser remelting coating has peeling at the corners and considerable local peelings in the center. Laser remelting mainly influences the thermal shock resistance of plasma sprayingAT13 coating by decreasing the initial failure resistance, decelerating crack propagation, and changing the failure mode of the coating.

Acknowledgments

We would like to express our sincere thanks to the Anhui Provincial Natural Science Foundation (2008085ME149), Anhui Provincial Top Academic Aid Program for Discipline (Major) Talents of Higher Education Institutions (gxbjZD2020087), Key Research and Development Project of Tongling City (20200201010), Anhui Provincial Natural Science Research Key Program of Higher Education Institutions (KJ2021A1052, KJ2021A1062), Jiangxi Key Laboratory of Forming and Joining Technology for Aerospace Components, Nanchang Hangkong University (EL202180264) and Academic Leader and Backup Candidate Research Project of Tongling University (2020tlxyxs02, 2020tlxyxs04) for funding this work. We would also like to thank 5th Annual International Workshop on Materials Science and Engineering (IWMSE2019). A partial earlier version of this paper was presented at the International Conference on IWMSE2019.

Data availability statement

All data that support the findings of this study are included within the article (and any supplementary files).

ORCID iDs

Dongsheng Wang https://orcid.org/0000-0003-2576-4288

References

[1] Diaz O G, Luna G G, Liao Z and Axinte D 2019 The new challenges of machining ceramic matrix composites (CMCs): review of surface integrity *Int. J. Mach. Tools Manuf* **139** 24–36
[2] Wang J C, Dommati H and Hsieh S J 2019 Review of additive manufacturing methods for high-performance ceramic materials *Int. J. Adv. Manuf. Technol.* **103** 2627–47
[3] Gonzalez-Gutierrez J, Cano S, Schuschnigg S, Kukla C, Sapkota J and Holzer C 2018 Additive manufacturing of metallic and ceramic components by the material extrusion of highly-filled polymers: a review and future perspectives *Materials* **11** 840
[4] Hu Y and Cong W 2018 A review on laser deposition-additive manufacturing of ceramics and ceramic reinforced metal matrix composites *Ceram. Int.* **44** 20599–612
[5] Zanurin A, Johari N A, Alias J, Ayu H M, Redzuan N and Izman S 2022 Research progress of sol-gel ceramic coating: a review *Mater. Today Proc.* **48** 1849–54
[6] Selvaraj S K, Srinivasan K, Deshmukh J, Agrawal D, Mungilwar S, Jagtap R and Hu Y C 2020 Performance comparison of advanced ceramic cladding approaches via solid-state and traditional welding processes: a review *Materials* **13** 5805
[7] Zhao L, Yao X, Hang R, Zhang X and Tang B 2018 Corrosion behavior of porous ZrO_2 ceramic coating on AZ31B magnesium alloy *Surf. Coat. Technol.* **349** 434–41
[8] Zhang D, Ge Y, Liu G, Gao F and Li P 2018 Investigation of tribological properties of micro-arc oxidation ceramic coating on Mg alloy under dry sliding condition *Ceram. Int.* **44** 16164–72

[9] Zavareh M A, Sarhan A A D M, Karimzadeh R, Singh R and Singh K 2018 Analysis of corrosion protection behavior of Al_2O_3-TiO_2 oxide ceramic coating on carbon steel pipes for petroleum industry *Ceram. Int.* **44** 5967–75

[10] Han R, Li J, Kong L, Liu J, Shan X, Cui X and Xiong T 2019 A novel phosphate-ceramic coating for high temperature oxidation resistance of Ti65 alloys *Ceram. Int.* **45** 23895–901

[11] Basha G M T, Srikanth A and Venkateshwarlu B 2020 A critical review on nano structured coatings for alumina-titania (Al_2O_3-TiO_2) deposited by air plasma spraying process (APS) *Mater. Today Proc.* **22** 1554–62

[12] Odhiambo J G, Li W, Zhao Y and Li C 2019 Porosity and its significance in plasma-sprayed coatings *Coatings* **9** 460

[13] Toma F L, Potthoff A, Berger L M and Leyens C 2015 Demands, potentials, and economic aspects of thermal spraying with suspensions: a critical review *J. Therm. Spray Technol.* **24** 1143–52

[14] Fauchais P, Vardelle M and Goutier S 2016 Latest researches advances of plasma spraying: from splat to coating formation *J. Therm. Spray Technol.* **25** 1534–53

[15] Vardelle A, Moreau C, Themelis N J and Chazelas C 2015 A perspective on plasma spray technology *Plasma Chem. Plasma Process.* **35** 491–509

[16] Afzal M, Ajmal M, Khan A N, Hussain A and Akhter R 2014 Surface modification of air plasma spraying WC–12% Co cermet coating by laser melting technique *Opt. Laser Technol.* **56** 202–6

[17] Yue T M, Xie H, Lin X, Yang H and Meng G 2013 Microstructure of laser re-melted AlCoCrCuFeNi high entropy alloy coatings produced by plasma spraying *Entropy* **15** 2833–45

[18] Ahmadi-Pidani R, Shoja-Razavi R, Mozafarinia R and Jamali H 2013 Laser surface modification of plasma sprayed CYSZ thermal barrier coatings *Ceram. Int.* **39** 2473–80

[19] Ghasemi R, Shoja-Razavi R, Mozafarinia R and Jamali H 2013 Laser glazing of plasma-sprayed nanostructured yttria stabilized zirconia thermal barrier coatings *Ceram. Int.* **39** 9483–90

[20] Wang Y, Li C, Guo L and Tian W 2010 Laser remelting of plasma sprayed nanostructured Al_2O_3–TiO_2 coatings at different laser power *Surf. Coat. Technol.* **204** 3559–66

[21] Wang Y, Li C G, Tian W and Yang Y 2009 Laser surface remelting of plasma sprayed nanostructured Al_2O_3–13wt% TiO_2 coatings on titanium alloy *Appl. Surf. Sci.* **255** 8603–10

[22] Zhang X C, Xu B S, Xuan F Z, Wang Z D and Tu S T 2011 Failure mode and fatigue mechanism of laser-remelted plasma-sprayed Ni alloy coatings in rolling contact *Surf. Coat. Technol.* **205** 3119–27

[23] Kulmala M and Vuoristo P 2008 Influence of process conditions in laser-assisted low-pressure cold spraying *Surf. Coat. Technol.* **202** 4503–8

[24] Serres N, Hlawka F, Costil S, Langlade C and Machi F 2011 Microstructures and mechanical properties of metallic NiCrBSi and composite NiCrBSi–WC layers manufactured via hybrid plasma/laser process *Appl. Surf. Sci.* **257** 5132–7

[25] Kadhim M J, Al-Rubaiey S I and Hammood A S 2013 The influence of laser specific energy on laser sealing of plasma sprayed yttria partially stabilized zirconia coating *Opt. Lasers Eng.* **51** 159–66

[26] Dyshlovenko S, Pierlot C, Pawlowski L, Tomaszek R and Chagnon P 2006 Experimental design of plasma spraying and laser treatment of hydroxyapatite coatings *Surf. Coat. Technol.* **201** 2054–60

[27] Dubourg L, Lima R S and Moreau C 2007 Properties of alumina–titania coatings prepared by laser-assisted air plasma spraying *Surf. Coat. Technol.* **201** 6278–84

[28] Kobylanska-Szkaradek K 2002 Laser-beam modification of oxide thermal barrier coatings deposited by plasma spraying in air *Lasers in Engineering* **12** 311–27

[29] Kobylańska–Szkaradek K 2006 Thermal barrier ZrO_2-Y_2O_3 obtained by plasma spraying method and laser melting *Journal of Achievements in Materials and Manufacturing Engineering* **17** 77–80

[30] Suutala J, Tuominen J and Vuoristo P 2006 Laser-assisted spraying and laser treatment of thermally sprayed coatings *Surf. Coat. Technol.* **201** 1981–7

[31] Schelz S, Branland N, Plessis D, Minot B and Guillet F 2006 Laser treatment of plasma-sprayed $ZrSiO_4$ coatings *Surf. Coat. Technol.* **200** 6384–8

[32] Shankar A R, Babu B J, Sole R, Mudali U K and Khatak H S 2007 Laser remelting of plasma sprayed zirconia based ceramic coating for pyrochemical reprocessing applications *Surf. Eng.* **23** 147–54

[33] Znamirowski Z, Pawlowski L, Cichy T and Czarczynski W 2004 Low macroscopic field electron emission from surface of plasma sprayed and laser engraved TiO_2, Al_2O_3 + 13TiO_2 and Al_2O_3 + 40TiO_2 coatings *Surf. Coat. Technol.* **187** 37–46

[34] Batista C, Portinha A, Ribeiro R M, Teixeira V, Costa M F and Oliveira C R 2005 Surface laser-glazing of plasma-sprayed thermal barrier coatings *Appl. Surf. Sci.* **247** 313–9

[35] Tondu S, Schnick T, Pawlowski L, Wielage B, Steinhäuser S and Sabatier L 2000 Laser glazing of FeCr–TiC composite coatings *Surf. Coat. Technol.* **123** 247–51

[36] Wong T T, Liang G Y, An G and MacAlpine J M K 2005 The electrical conductivity of laser-remelted and plasma-sprayed Ni and Cr coatings *J. Mater. Process. Technol.* **159** 265–71

[37] Sidhu B S, Puri D and Prakash S 2004 Characterisations of plasma sprayed and laser remelted NiCrAlY bond coats and Ni_3Al coatings on boiler tube steels *Mater. Sci. Eng. A* **368** 149–58

[38] Dyshlovenko S, Pawlowski L, Smurov I and Veiko V 2006 Pulsed laser modification of plasma-sprayed coatings: Experimental processing of hydroxyapatite and numerical simulation *Surf. Coat. Technol.* **201** 2248–55

[39] Sidhu B S, Puri D and Prakash S 2005 Mechanical and metallurgical properties of plasma sprayed and laser remelted Ni–20Cr and Stellite-6 coatings *J. Mater. Process. Technol.* **159** 347–55

[40] Pokhmurska A and Ciach R 2000 Microstructure and properties of laser treated arc sprayed and plasma sprayed coatings *Surf. Coat. Technol.* **125** 415–8

[41] Batista C, Portinha A, Ribeiro R M, Teixeira V, Costa M F and Oliveira C R 2006 Morphological and microstructural characterization of laser-glazed plasma-sprayed thermal barrier coatings *Surf. Coat. Technol.* **200** 2929–37

[42] Chen C, Wang D, Bao Q, Zhang L and Lei T 2005 Influence of laser remelting on the microstructure and phases constitution of plasma sprayed hydroxyapatite coatings *Appl. Surf. Sci.* **250** 98–103

[43] Antou G, Montavon G, Hlawka F, Cornet A, Coddet C and Machi F 2003 Modification of ceramic thermal spray deposit microstructures implementing *in situ* laser remelting *Surf. Coat. Technol.* **172** 279–90

[44] Tomaszek R, Pawlowski L, Zdanowski J, Grimblot J and Laureyns J 2004 Microstructural transformations of TiO_2, Al_2O_3 + 13TiO_2 and Al_2O_3 + 40TiO_2 at plasma spraying and laser engraving *Surf. Coat. Technol.* **185** 137–49

[45] Krishnan R, Dash S, Kesavamoorthy R, Rao C B, Tyagi A K and Raj B 2006 Laser surface modification and characterization of air plasma sprayed alumina coatings *Surf. Coat. Technol.* **200** 2791–9

[46] Ouyang J H and Sasaki S 2002 Microstructure and tribological characteristics of ZrO_2–Y_2O_3 ceramic coatings deposited by laser-assisted plasma hybrid spraying *Tribol. Int.* **35** 255–64
[47] Zhu C, Li P, Javed A, Liang G Y and Xiao P 2012 An investigation on the microstructure and oxidation behavior of laser remelted air plasma sprayed thermal barrier coatings *Surf. Coat. Technol.* **206** 3739–46
[48] Kromer R, Costil S, Verdy C, Gojon S and Liao H 2018 Laser surface texturing to enhance adhesion bond strength of spray coatings–Cold spraying, wire-arc spraying, and atmospheric plasma spraying *Surf. Coat. Technol.* **352** 642–53
[49] Kromer R, Costil S, Cormier J, Courapied D, Berthe L, Peyre P and Boustie M 2015 Laser surface patterning to enhance adhesion of plasma sprayed coatings *Surf. Coat. Technol.* **278** 171–82
[50] Mateos J J M E, Cuetos J M, Fernandez E and Vijande R 2000 Tribological behaviour of plasma-sprayed WC coatings with and without laser remelting *Wear* **239** 274–81
[51] Szkodo M, Bień A and Antoszkiewicz M 2016 Effect of plasma sprayed and laser re-melted Al_2O_3 coatings on hardness and wear properties of stainless steel *Ceram. Int.* **42** 11275–84
[52] Liang G Y, Wong T T, MacAlpine J M K and Su J Y 2000 A study of wear resistance of plasma-sprayed and laser-remelted coatings on aluminium alloy *Surf. Coat. Technol.* **127** 232–7
[53] Yuanzheng Y, Youlan Z, Zhengyi L and Yuzhi C 2000 Laser remelting of plasma sprayed Al_2O_3 ceramic coatings and subsequent wear resistance *Mater. Sci. Eng. A* **291** 168–72
[54] Mateos J, Cuetos J M, Vijande R and Fernandez E 2001 Tribological properties of plasma sprayed and laser remelted 75/25 Cr_3C_2/NiCr coatings *Tribol. Int.* **34** 345–51
[55] Gao Y L, Wang C S, Yao M and Liu H B 2007 The resistance to wear and corrosion of laser-cladding Al_2O_3 ceramic coating on Mg alloy *Appl. Surf. Sci.* **253** 5306–11
[56] Navas C, Vijande R, Cuetos J M, Fernández M R and De Damborenea J 2006 Corrosion behaviour of NiCrBSi plasma-sprayed coatings partially melted with laser *Surf. Coat. Technol.* **201** 776–85
[57] Batista C, Portinha A, Ribeiro R M, Teixeira V and Oliveira C R 2006 Evaluation of laser-glazed plasma-sprayed thermal barrier coatings under high temperature exposure to molten salts *Surf. Coat. Technol.* **200** 6783–91
[58] Ahmadi-Pidani R, Shoja-Razavi R, Mozafarinia R and Jamali H 2014 Improving the hot corrosion resistance of plasma sprayed ceria–yttria stabilized zirconia thermal barrier coatings by laser surface treatment *Mater. Des.* **57** 336–41
[59] Ghasemi R, Shoja-Razavi R, Mozafarinia R, Jamali H, Hajizadeh-Oghaz M and Ahmadi-Pidani R 2014 The influence of laser treatment on hot corrosion behavior of plasma-sprayed nanostructured yttria stabilized zirconia thermal barrier coatings *J. Eur. Ceram. Soc.* **34** 2013–21
[60] Wu Y N, Zhang G, Feng Z C, Zhang B C, Liang Y and Liu F J 2001 Oxidation behavior of laser remelted plasma sprayed NiCrAlY and NiCrAlY–Al_2O_3 coatings *Surf. Coat. Technol.* **138** 56–60
[61] Ahmadi-Pidani R, Shoja-Razavi R, Mozafarinia R and Jamali H 2012 Improving the thermal shock resistance of plasma sprayed CYSZ thermal barrier coatings by laser surface modification *Opt. Lasers Eng.* **50** 780–6
[62] Ghasemi R, Shoja-Razavi R, Mozafarinia R and Jamali H 2014 The influence of laser treatment on thermal shock resistance of plasma-sprayed nanostructured yttria stabilized zirconia thermal barrier coatings *Ceram. Int.* **40** 347–55
[63] Lee J H, Tsai P C and Chang C L 2008 Microstructure and thermal cyclic performance of laser-glazed plasma-sprayed ceria–yttria-stabilized zirconia thermal barrier coatings *Surf. Coat. Technol.* **202** 5607–12
[64] Wang Y, Darut G, Poirier T, Stella J, Liao H and Planche M P 2017 Ultrasonic cavitation erosion of as-sprayed and laser-remelted yttria stabilized zirconia coatings *J. Eur. Ceram. Soc.* **37** 3623–30
[65] Yılmaz R, Kurt A O, Demir A and Tatlı Z 2007 Effects of TiO_2 on the mechanical properties of the Al_2O_3–TiO_2 plasma sprayed coating *J. Eur. Ceram. Soc.* **27** 1319–23
[66] Jia S K, Yong Z O U, Xu J Y, Jing W A N G and Lei Y U 2015 Effect of TiO_2 content on properties of Al_2O_3 thermal barrier coatings by plasma spraying *Transactions of Nonferrous Metals Society of China* **25** 175–83
[67] Vargas F, Ageorges H, Fournier P, Fauchais P and López M E 2010 Mechanical and tribological performance of Al_2O_3–TiO_2 coatings elaborated by flame and plasma spraying *Surf. Coat. Technol.* **205** 1132–6
[68] Basha G M T, Srikanth A and Venkateshwarlu B 2020 A critical review on nano structured coatings for alumina-titania (Al_2O_3–TiO_2) deposited by air plasma spraying process (APS) *Mater. Today Proc.* **22** 1554–62
[69] Basha G M T, Srikanth A and Venkateshwarlu B 2020 Effect of reinforcement of carbon nanotubes on air plasma sprayed conventional Al_2O_3-3% TiO_2 ceramic coatings *Mater. Today Proc.* **20** 191–4
[70] Sahab A R M, Saad N H, Kasolang S and Saedon J 2012 Impact of plasma spray variables parameters on mechanical and wear behaviour of plasma sprayed Al_2O_3 3% wt TiO_2 coating in abrasion and erosion application *Procedia Engineering* **41** 1689–95
[71] Song E P, Ahn J, Lee S and Kim N J 2008 Effects of critical plasma spray parameter and spray distance on wear resistance of Al_2O_3–8 wt% TiO_2 coatings plasma-sprayed with nanopowders *Surf. Coat. Technol.* **202** 3625–32
[72] Song E P, Ahn J, Lee S and Kim N J 2006 Microstructure and wear resistance of nanostructured Al_2O_3–8wt% TiO_2 coatings plasma-sprayed with nanopowders *Surf. Coat. Technol.* **201** 1309–15
[73] Manaee P, Valefi Z and Goodarz M 2020 The effect of bond coat type on the stab resistance of Al_2O_3–13 wt% TiO_2 plasma sprayed ceramic coating on aramid fabrics *Surfaces and Interfaces* **18** 100432
[74] Wang M, Zhou Z, Yi Y and Wang Z 2019 Thermal-shock resistance of plasma sprayed Al_2O_3-13 wt% TiO_2 coating evaluated by residual strength method *Surf. Coat. Technol.* **375** 888–93
[75] Mehar S, Sapate S G, Vashishtha N and Bagde P 2020 Effect of Y_2O_3 addition on tribological properties of plasma sprayed Al_2O_3-13% TiO_2 coating *Ceram. Int.* **46** 11799–810
[76] Sure J, Shankar A R, Upadhyay B N and Mudali U K 2012 Microstructural characterization of plasma sprayed Al_2O_3-40 wt% TiO_2 coatings on high density graphite with different post-treatments *Surf. Coat. Technol.* **206** 4741–9
[77] Richter A, Berger L M, Sohn Y J, Conze S, Sempf K and Vaßen R 2019 Impact of Al_2O_3-40 wt% TiO_2 feedstock powder characteristics on the sprayability, microstructure and mechanical properties of plasma sprayed coatings *J. Eur. Ceram. Soc.* **39** 5391–402
[78] Kang J J, Xu B S, Wang H D and Wang C B 2013 Influence of spraying parameters on the microstructure and properties of plasma-sprayed Al_2O_3/40% TiO_2 coating *Phys. Proc.* **50** 169–76
[79] He X, Song P, Yu X, Li C, Huang T, Zhou Y, Li Q, Lü K, Lü J and Lu J 2018 Evolution of cracks within an Al_2O_3–40 wt% TiO_2/NiCoCrAl gradient coating *Ceram. Int.* **44** 20798–807
[80] Friis M, Persson C and Wigren J 2001 Influence of particle in-flight characteristics on the microstructure of atmospheric plasma sprayed yttria stabilized ZrO_2 *Surf. Coat. Technol.* **141** 115–27
[81] Jafarzadeh K, Valefi Z and Ghavidel B 2010 The effect of plasma spray parameters on the cavitation erosion of Al_2O_3–TiO_2 coatings *Surf. Coat. Technol.* **205** 1850–5

[82] Li C J, Yang G J and Ohmori A 2006 Relationship between particle erosion and lamellar microstructure for plasma-sprayed alumina coatings *Wear* **260** 1166–72
[83] Lathabai S, Ottmüller M and Fernandez I 1998 Solid particle erosion behaviour of thermal sprayed ceramic, metallic and polymer coatings *Wear* **221** 93–108
[84] Tsai P C, Lee J H and Chang C L 2007 Improving the erosion resistance of plasma-sprayed zirconia thermal barrier coatings by laser glazing *Surf. Coat. Technol.* **202** 719–24
[85] Rangaraj S and Kokini K 2004 Fracture in single-layer zirconia (YSZ)–bond coat alloy (NiCoCrAlY) composite coatings under thermal shock *Acta Mater.* **52** 455–65
[86] Mesrati N, Saif Q, Treheux D, Moughil A, Fantozzi G and Vincent A 2004 Characterization of thermal fatigue damage of thermal barrier produced by atmospheric plasma spraying *Surf. Coat. Technol.* **187** 185–93
[87] Khan A N and Lu J 2007 Thermal cyclic behavior of air plasma sprayed thermal barrier coatings sprayed on stainless steel substrates *Surf. Coat. Technol.* **201** 4653–8
[88] Loghman-Estarki M R, Razavi R S, Edris H and Jamali H 2014 Life time of new SYSZ thermal barrier coatings produced by plasma spraying method under thermal shock test and high temperature treatment *Ceram. Int.* **40** 1405–14